Generalized Transition State Theory. Bond Energy–Bond Order Method for Canonical Variational Calculations with Application to Hydrogen Atom Transfer Reactions

Bruce C. Garrett and Donald G. Truhlar*

Contribution from the Department of Chemistry, University of Minnesota, Minneapolis, Minnesota 55455. *Received February 2, 1979*

Abstract: A formalism for canonical variational theory calculations on atom–diatom reactions with linear generalized transition states is presented. Anharmonicity is included in both stretches and bend.0 A set of 36 realistic potential energy surfaces is generated by an extended and modified bond energy–bond order method. The canonical variational formalism is applied using these surfaces and the resulting thermal rate constants are compared to those predicted by conventional transition-state theory for the same reactions. The median ratio of the conventionally calculated rate to the canonical variational one increases from 1.6 at 200 K to 2.0 at 2400 K. The error is generally larger for reactions with symmetric saddle points and for those with very asymmetric saddle points. Ten representative reactions are discussed in detail to illustrate the competition and reinforcement of various factors in determining the location of the generalized transition state and the effect of varying this location.

Introduction

While the usefulness of transition-state theory for the prediction and correlation of gas-phase chemical reaction rates is well established,[1-4] the magnitude and nature of the errors caused by the transition-state formulation are still largely uncertain. In this article we attempt to study these errors by applying conventional transition-state theory and the canonical variational theory of reaction rates to a representative series of models of three-body hydrogen atom transfer reactions.

The fundamental assumption of classical transition-state theory is that trajectories do not recross the transition state dividing surface separating reactants from products.[5-7] Conventionally the dividing surface is located at the saddle point of the potential energy surface, but in generalized transition-state theory it may be located anywhere. If the fundamental assumption is valid, then classical transition-state theory is exact for the classical equilibrium reaction rate; if it is false then classical transition-state theory overestimates the classical equilibrium reaction rate.[7] This provides the basis for classical variational transition-state theories in which the location of the dividing surface is varied to minimize the calculated rate constant.[8-10] In a classical world the breakdown of the fundamental assumption becomes more severe at higher temperatures.[9-11]

For real reactions the effects of zero-point energies and quantized energy levels and dynamic quantum effects are usually large. In a quantum-mechanical world transition-state theory does not provide an upper bound to the equilibrium rate. Nevertheless we have applied variational transition-state theory with quantized partition functions and quantum-mechanical effects on reaction-coordinate motion to collinear reactions of hydrogen molecules and have shown that the predictions of conventional and variational transition-state theory sometimes differ significantly.[12,13] Furthermore, comparison to accurate quantum-mechanical calculations[14] of the collinear rate constants for assumed potential energy surfaces shows that the variational minimization of the calculated rate constant with respect to location of the dividing surface often provides significant improvement even when quantum effects must be included.[12,15]

In this article we attempt to learn whether the predictions of conventional and variational transition-state theories differ significantly for reactions in three dimensions. Since accurate potential energy surfaces are available for very few reactions, we base our calculations on a simple but realistic model for potential energy surfaces, namely, the bond energy–bond order (BEBO) model.[1,16] Although this model does not predict quantitatively reliable potential energy surfaces, it does predict realistic ones. We use the BEBO model to generate a whole series of potential energy surfaces so that we may study the variational transition-state theory effects for a variety of reaction types. In each case we calculate rate constants by both conventional transition-state theory and variational transition-state theory. The version of variational transition-state theory we employ is the canonical variational method, which is equivalent to the maximization[3,13] of the free energy of activation.[17] Since the canonical variational theory has been shown[12] to predict more reliable quantum mechanical rate constants for collinear reactions where the accurate rates for given potential energy surfaces are available, we regard it as more reliable in three dimensions too. Thus we use the deviation of the conventional transition-state theory calculations from the canonical variational ones as a measure of the inaccuracy of the former. We find large deviations for some classes of reactions, and we recommend the canonical variational theory as the most reliable theory available for the practical computation of gas-phase reaction rate constants.

Theory

Canonical Variational Transition-State Theory. In this paper we consider reactions of an atom A and a diatomic molecule BC for a class of reactions in which the minimum-energy reaction path is collinear. Conventional transition-state theory provides the following expression for the canonical rate constant (i.e., the rate constant for a canonical ensemble characterized by a temperature T):

$$k^{\ddagger}(T) = \sigma\kappa(T)\frac{k_B T}{h}\frac{Q^{\ddagger}(T)}{\Phi^{R}(T)}\exp(-V^{\ddagger}/k_B T) \qquad (1)$$

where σ is a statistical symmetry factor (discussed below), $\kappa(T)$ is the transmission coefficient, k_B is Boltzmann's constant, h is Planck's constant, $Q^{\ddagger}(T)$ is the transition-state partition function, $V^{\ddagger}$ is the potential energy at the saddle point where the zero of energy is the bottom of the BC potential well with A infinitely separated, and $\Phi^{R}(T)$ is the reactants' partition function per unit volume. The latter is approximated as

$$\Phi^{R}(T) = \Phi_{rel}^{A,BC}(T)Q_{str}^{BC}(T)Q_{r}^{BC}(T) \qquad (2)$$

where $\Phi_{rel}^{A,BC}$ is the relative translational partition function per unit volume for reactants

$$\Phi_{rel}^{A,BC}(T) = (2\pi\mu k_B T/h^2)^{3/2} \qquad (3)$$

μ is the reduced mass for relative translational energy, $Q_{str}^{BC}(T)$ is the vibrational partition function for BC

0002-7863/79/1501-4534$01.00/0

$$Q_{str}^{BC}(T) = \sum_{n=0}^{n_{max}} \exp(-\epsilon_{str,n}^{BC}/k_BT) \quad (4)$$

$\epsilon_{str,n}^{BC}$ is the vibrational energy of BC with vibrational quantum number n. Q_r^{BC} is the rotational partition function for BC

$$Q_r^{BC}(T) = \sum_{j=0}^{\infty} (2j+1) \exp(-\epsilon_{r,j}^{BC}/k_BT) \quad (5)$$

$\epsilon_{r,j}^{BC}$ is the rotational energy of BC with rotational quantum number j

$$\epsilon_{r,j}^{BC} = \hbar^2 j(j+1)/[2\mu_{BC}(r_e^{BC})^2] \quad (6)$$

μ_{BC} is the diatomic reduced mass, and r_e^{BC} is the equilibrium internuclear separation of the BC molecule. The transition-state partition function is approximated as

$$Q^{\ddagger}(T) = Q_{str}^{\ddagger}(T)[Q_b^{\ddagger}(T)]^2 Q_r^{\ddagger}(T) \quad (7)$$

where $Q_{str}^{\ddagger}(T)$, $Q_b^{\ddagger}(T)$, and $Q_r^{\ddagger}(T)$ are the transition-state partition functions for the stretching vibration, for bending, and for rotation, respectively. Note that the zero of energy for $\Phi^R(T)$ is the same as for the potential energy but the zero of energy for $Q^{\ddagger}(T)$ is at the saddle point.

The statistical symmetry factor σ in eq 1 and 12 arises from the indistinguishability of like atoms. The proper evaluation of σ has been the subject of much discussion,[18] but the simplest correct prescription is given by Weston and Schwarz.[19] In their treatment, symmetry numbers are omitted from all rotational partition functions as indicated in eq 5 and 16; this is equivalent to treating all atoms as distinguishable. Then σ is just the "reaction path multiplicity" or the number of equivalent reaction paths from reactants to products. Therefore, in the reaction of an atom with a homonuclear diatom, $\sigma = 2$, and the resulting rate constant is the sum of the reaction rate with both ends of the diatom. For reaction of atoms with heteronuclear diatoms, $\sigma = 1$.

To facilitate generalization of the theory to a variationally located dividing surface it is convenient to introduce coordinates

$$x = r_{AB} + c_1 r_{BC} \quad (8)$$

and

$$y = c_2 r_{BC} \quad (9)$$

where

$$c_1 = \frac{m_C}{m_B + m_C} \quad (10)$$

and

$$c_2 = \sqrt{\frac{\mu_{BC}}{\mu}} \quad (11)$$

such that collinear dynamics are equivalent to the motion of a mass point of mass μ moving in the (x, y) plane. The minimum-energy path (MEP) is the path of steepest descents in the (x, y) plane from the saddle point toward reactants and products. The reaction coordinate s is the signed distance along the MEP from the saddle point. Notice that the scaled and skewed coordinates (x, y) defined above are but one set out of an infinite number of coordinate systems which reduce the collinear dynamics to motion of a mass point. However, as discussed elsewhere,[12] the path of steepest descent is the same in all such systems. In canonical variational transition-state theory one varies the location of the dividing surface to minimize the canonical rate constant. In the present article we minimize with respect to a limited set of dividing surfaces, namely, ones which are orthogonal in the (x, y) plane to the minimum-energy path. These surfaces are parametrically characterized by the value of s where they intersect this path.

Thus we define a generalized transition state for each location s of this surface. The generalized transition-state-theory expression for the canonical rate constant, neglecting the transmission coefficient, is given by

$$k^{GT}(T,s) = \sigma \frac{k_BT}{h} \frac{Q^{GT}(T,s)}{\Phi^R(T)} \exp[-V_{MEP}(s)/k_BT] \quad (12)$$

where $V_{MEP}(s)$ is the potential energy at a point s on the MEP and $Q^{GT}(T,s)$ is the partition function for the generalized transition state at s given in terms of generalized transition-state stretching, bending, and rotational partition functions by

$$Q^{GT}(T,s) = Q_{str}^{GT}(T,s)[Q_b^{GT}(T,s)]^2 Q_r^{GT}(T,s) \quad (13)$$

where

$$Q_{str}^{GT}(T,s) = \sum_{n=0}^{n_{max}(s)} \exp[-\epsilon_{str,n}^{GT}(s)/k_BT] \quad (14)$$

$$Q_b^{GT}(T,s) = \sum_{i=0}^{\infty} \exp[-\epsilon_{b,i}^{GT}(s)/k_BT] \quad (15)$$

$$Q_r^{GT}(T,s) = \sum_{J=0}^{\infty} (2J+1) \exp[-\epsilon_{r,J}^{GT}(s)/k_BT] \quad (16)$$

$$\epsilon_{r,J}^{GT}(s) = \hbar^2 J(J+1)/[2I(s)] \quad (17)$$

$$I(s) = \{[r_{AB}(s)]^2 m_A m_{BC} + [r_{BC}(s)]^2 m_C m_{AB} + [2r_{AB}(s) r_{BC}(s)] m_A m_C\}/m_{ABC} \quad (18)$$

$\epsilon_{str,n}^{GT}(s)$ is the vibrational energy for the bound stretching vibration of the generalized transition state with vibrational quantum number n, and $\epsilon_{b,i}^{GT}(s)$, $\epsilon_J^{GT}(s)$, and $I(s)$ are the bending vibrational energy with quantum number i, the rotational energy with quantum number J, and the moment of inertia of the linear triatomic generalized activated complex at s. The Boltzmann factor in eq 13 arises because the zero of energy for $Q^{GT}(T,s)$ is taken as the bottom of the vibrational well at s.

Conventional transition-state theory is obtained by evaluating (12) at $s = 0$ and canonical variational theory is obtained by minimizing the calculated rate with respect to s:

$$k^{CVT}(T) = \min_s k^{GT}(T,s) \quad (19)$$

The value of the reaction coordinate at which this minimum occurs is called $s_*^{CVT}(T)$. Canonical variational theory is identical with the criterion of maximum free energy of activation. Generalizing the thermodynamic formulation of transition-state theory gives

$$k^{GT}(T,s) = \frac{k_BT}{h} K^0 e^{-\Delta G^{GT,0}(T,s)/RT} \quad (20)$$

where K^0 is the reciprocal of the standard-state concentration (taken here as 1 cm^3 molecule^{-1}), $\Delta G^{GT,0}(T,s)$ is the generalized free energy of activation, and R is the gas constant. Minimization of $k^{GT}(T,s)$ is then equivalent to maximizing the free-energy change $\Delta G^{GT,0}(T,s)$.

Next we discuss in more detail our model for evaluating $Q^{GT}(T,s)$. The stretching vibrational coordinate, u^s, is defined at any location s along the MEP as being normal to the reaction coordinate in the (x, y) plane. The coordinate z^s is tangent to the reaction coordinate at the location s. The coordinates (z^s, u^s) then provide an orthogonal system related to (x, y) by a rotation. The energy levels $\epsilon_{str,n}^{GT}(s)$ in eq 14 are then the eigenvalues of the one-dimensional potential $V(z^s = 0, u^s)$. Notice that this procedure automatically leads to

$$\epsilon_{str,n}^{BC} = \epsilon_{str,n}^{GT}(s = -\infty) \quad (21a)$$

$$\epsilon_{str,n}^{AB} = \epsilon_{str,n}^{GT}(s = +\infty) \quad (21b)$$

and

$$\epsilon_{str,n}^{\ddagger} = \epsilon_{str,n}^{GT}(s = 0) \quad (22)$$

A good model is to fit the vibrational potentials to Morse functions

$$V(z^s = 0, u^s) = V_{MEP}(s) + D_e(s)\{1 - \exp[-a_M(s)u^s]\}^2 \quad (23)$$

in which case the energy levels referred to $V_{MEP}(s)$ are

$$\epsilon_{str,n}^{GT}(s) = \hbar\omega_e(s)[(n + 1/2) - x_e(s)(n + 1/2)^2] \quad (24)$$

where

$$\omega_e(s) = a_M(s)[2D_e(s)/\mu]^{1/2} \quad (25)$$

$$x_e(s) = \hbar a_M(s)[8\mu D_e(s)]^{-1/2} \quad (26)$$

Note that in the harmonic approximation

$$V(z^s = 0, u^s) \simeq V_{MEP}(s) + 1/2F_{u^s}(s)(u^s)^2 \quad (27)$$

where $F_{u^s}(s)$ is the force constant for the transverse vibration and

$$\omega_e(s) = [\mu^{-1}F_{u^s}(s)]^{1/2} \quad (28)$$

Thus in order for the Morse potential to have the correct harmonic force constant it is required that

$$a_M(s) = \{F_{u^s}(s)/[2D_e(s)]\}^{1/2} \quad (29)$$

A reasonable approximation for the bending potential is a mixed harmonic-quartic potential[20,21]

$$\Delta V_b(\Phi,s) = 1/2F_\Phi(s)(\Phi - \pi)^2 + \frac{1}{24}A_\Phi(s)(\Phi - \pi)^4 \quad (30)$$

where Φ is the bond angle. The effective mass for this degree of freedom is given by the Wilson G matrix element[22]

$$m_\Phi(s) = G_{\Phi\Phi}^{-1}(s) \quad (31)$$

where

$$G_{\Phi\Phi}(s) = \frac{1}{m_A[r_{AB}(s)]^2} + \frac{1}{m_C[r_{BC}(s)]^2} + \frac{1}{m_B}\left[\frac{1}{r_{AB}(s)} + \frac{1}{r_{BC}(s)}\right]^2 \quad (32)$$

The harmonic frequency for this degree of freedom is then

$$\omega_b(s) = [G_{\Phi\Phi}(s)F_\Phi(s)]^{1/2} \quad (33)$$

Approximate energy levels for the mixed harmonic-quartic oscillator may be determined by a perturbation-variation method which yields[23]

$$\epsilon_{b,i}^{GT}(s) = 1/2(\lambda_s^2 + \lambda_s^{-2})\epsilon_{b,i}^0(s) + \frac{1}{24}A_\Phi(s)\lambda_s^{-4}\epsilon_{b,i}^1(s) \quad (34)$$

where

$$\epsilon_{b,i}^0(s) = \hbar\omega_b(s)(i + 1/2) \quad (35)$$

$$\epsilon_{b,i}^1(s) = \frac{3\hbar^2}{4[m_\Phi(s)\omega_b(s)]^2}(2i^2 + 2i + 1) \quad (36)$$

and λ_s is determined by solving

$$\lambda_s^6 - \lambda_s^2 - \frac{1}{6}A_\Phi(s)[\epsilon_{b,i}^1(s)/\epsilon_{b,i}^0(s)] = 0 \quad (37)$$

The transmission coefficient $\kappa(T)$ in principle accounts for all deficiencies of transition-state theory, thereby yielding the exact quantum-mechanical rate constant. However, the evaluation of this exact transmission coefficient is equivalent to an exact solution to the collision problem and is impractical. In this paper we used two simple prescriptions for $\kappa(T)$. The first is to set it to unity. Secondly, we used the lowest order Wigner tunneling correction[24]

$$\kappa^W(T) = 1 + \frac{1}{24}\left|\frac{\hbar\omega^{\ddagger}}{k_BT}\right|^2 \quad (38)$$

where $\omega^{\ddagger}$ is the imaginary frequency for the reaction coordinate motion across the saddle point and is defined by

$$\omega^{\ddagger} = [\mu^{-1}F_s(s = 0)] \quad (39)$$

where

$$F_s(s = 0) = \left(\frac{\partial^2 V}{\partial z^{s2}}\right)_{u^s}\Bigg|_{s=0,u^s=0} \quad (40)$$

Although the assumptions behind the derivation of eq 38 are seldom satisfied,[7,25] we have found empirically that it is often as reliable as much more sophisticated methods for estimating tunneling effects.[12,25] In the present study the emphasis is on the location of the dividing surface and we evaluate $\kappa(T)$ only to obtain an indication of whether tunneling corrections are significant or negligible for the various examples considered. For this purpose the Wigner method provides an adequate indication.

Bond Energy-Bond Order Method. To evaluate the generalized transition-state theory rate expression, eq 12 and following, it is necessary to have certain information about the potential energy surface. At present, this information is not generally available. In this section we show, however, that all the information needed can be estimated by the bond energy-bond order (BEBO) method.[1,16] Details of the BEBO method and its applications to conventional transition-state theory are given elsewhere;[1,16,26-28] however, our application requires an extension of the method. Further, our techniques differ from those found in the literature even for the case of conventional transition-state theory.

The quantitative predictions of the BEBO model are sensitive to the input data and not generally quantitatively reliable.[29] However, the method does produce physically reasonable potential surfaces for many systems which are not ionic.[30,31] Our motivation for using the BEBO method for a range of systems is not that we expect it to be quantitatively accurate for any of these systems but rather that in this way we generate a range of realistic potential energy surfaces which can be used to gauge the nature and magnitude of generalized transition-state effects. The parameters required by the BEBO method are the dissociation energy D_e^{XY}, equilibrium internuclear distance r_e^{XY}, and Morse parameter a_M^{XY} for XY = AB, BC, and AC and the bond order parameter p^{XY} for XY = AB and BC. For our purposes it is not necessary to use the most accurate values so we used values of ref 16 whenever possible. In a few cases the required values are not given in ref 16; the values used[28,32-34] in those cases are given in ref 21. The BEBO method is most appropriate for atom transfer between two singly valent doublet atoms or radicals. Thus the electronic structures of the three-atom model reactions considered in the present BEBO model do not always correspond closely to those for the actual three-atom system. For example, the C + HC model considered here is a better prototype for the C-H-C portion of the $H_3C + HCH_3$ reaction than it is for $C(^3P) + HC(^2\Pi)$. In the present work, though, the BEBO potential surface for C + HC serves as a model of one possible realistic kind of potential for a three-atom reaction.

In the BEBO method, configurations along the MEP are assumed to be collinear and given by

$$r_{AB}(s) = r_e^{AB} - P \ln n_{AB}(s) \quad (41)$$

$$r_{BC}(s) = r_e^{BC} - P \ln n_{BC}(s) \quad (42)$$

$$r_{AC}(s) = r_{AB}(s) + r_{BC}(s) \quad (43)$$

$$n_{AB}(s) + n_{BC}(s) = 1 \tag{44}$$

where $r_{XY}(s)$ and $n_{XY}(s)$ are internuclear separations and bond orders, respectively, along the minimum-energy path and P is the Pauling parameter (assumed here to be 0.26 Å as in ref 1 and 16). BEBO does not specify whether the MEP given by eq 41–43 is the path of steepest descents in the (r_{AB}, r_{BC}) coordinate system or in a scaled and skewed coordinate system such as (x, y). For convenience in calculating the transverse vibrational energies, we assume that it is the MEP in the (x, y) coordinate system. The equations for the MEP in the (x, y) coordinate system are obtained from eq 8–11, 41, 42, and 44

$$x(s) = r_e^{AB} + c_1 r_e^{BC} - P(\ln \{n_{AB}(s)[1 - n_{AB}(s)]^{c_1}\}) \tag{45}$$

$$y(s) = c_2 r_e^{BC} - P \ln [1 - n_{AB}(s)]^{c_2} \tag{46}$$

where $x(s)$ and $y(s)$ are the coordinates of points on the MEP. Notice that the bond order, $n_{AB}(s)$, is in 1:1 correspondence with s and it can be viewed as an alternative progress variable. The reaction coordinate varies from $-\infty$ to ∞, but $n_{AB}(s)$ varies from 0 to 1.

The rest of the BEBO model follows from three additional assumptions. (1) The value of the potential energy along the MEP is given by

$$V_{MEP}(s) = V_{bond}^{AB}(s) + V_{bond}^{BC}(s) + V_{AM}^{AC}[r_{AC}(s)] - D_e^{BC} \tag{47}$$

where the final term fixes the zero of energy at the bottom of the reactant potential well; the bonding term is

$$V_{bond}^{XY}(s) = D_e^{XY}[n_{XY}(s)]^{p^{XY}} \tag{48}$$

and the anti-Morse antibonding potential is

$$V_{AM}^{AC}(r) = {}^1/_4 D_e^{AC}\{1 + \exp[-a_M^{AC}(r - r_e^{AC})]\}^2 - {}^1/_4 D_e^{AC} \tag{49}$$

Using eq 41–44, eq 49 can be written

$$V_{AM}^{AC}[r_{AC}(s)] = D_e^{AC} Bm(s)[1 + Bm(s)] \tag{50}$$

where

$$B = {}^1/_2 \exp[a_M^{AC}(r_e^{AC} + r_e^{AB} - r_e^{BC})] \tag{51}$$

$$m(s) = \{n_{AB}(s)[1 - n_{AB}(s)]\}^{P a_M^{AC}} \tag{52}$$

(2) For a bent geometry with (r_{AB}, r_{BC}) the same as some point $[r_{AB}(s), r_{BC}(s)]$ on the collinear MEP, the potential is given by (47) except with the actual value of r_{AC} instead of the value given in (43). Since $V_{AM}^{AC}(r)$ is a repulsive interaction, the energy always increases on bending from the MEP, as required for consistency. (3) For collinear configurations near but not on the MEP, the potential energy difference from the MEP may be computed by the following modified Badger's rule:

$$dV = {}^1/_2 n_{AB}(s) F^{AB}(dr_{AB})^2 + {}^1/_2 n_{BC}(s) F^{BC}(dr_{BC})^2 + {}^1/_2 \left(\frac{\partial^2 V_{AM}^{AC}}{\partial r^2}\right)_{n_{AB}(s), n_{BC}(s)} (dr_{AC})^2 \tag{53}$$

where F^{XY} is the force constant of the diatomic XY given by

$$F^{XY} = 2(a_M^{XY})^2 D_e^{XY} \tag{54}$$

Using these assumptions we can obtain all the parameters needed for the generalized transition-state theory calculation using eq 12–18 and 21–40. We perform conventional transition-state theory calculations by setting $s = 0$ in these equations; canonical variational theory is obtained by applying (19).

The Morse parameters for eq 23 are obtained as follows. The dissociation energy is obtained from (47):

$$D_e(s) = D_e^{BC} - V_{MEP}(s) \tag{55}$$

The coordinates (u^s, z^s) are defined, for a fixed value of s, to be normal and tangent to the MEP, respectively. The tangent to the minimum energy path can be obtained from eq 45 and 46 and the relationship

$$\frac{dy(s)}{dx(s)} = \frac{dy(s)/dn_{AB}(s)}{dx(s)/dn_{AB}(s)} \tag{56}$$

which yields

$$\frac{dy(s)}{dx(s)} = -\frac{c_2 n_{AB}(s)}{1 - (1 + c_1) n_{AB}(s)} \tag{57}$$

Then (z^s, u^s) are defined by

$$z^s = [x - x(s)] \cos\theta(s) + [y - y(s)] \sin\theta(s) \tag{58}$$

$$u^s = -[x - x(s)] \sin\theta(s) + [y - y(s)] \cos\theta(s) \tag{59}$$

where

$$\theta(s) = \tan^{-1}\left(\frac{dy(s)}{dx(s)}\right) \tag{60}$$

The potential energy for the transverse stretching vibration at any location along the MEP is given by eq 53 with z^s held fixed. The infinitesimal changes in r_{AB}, r_{BC}, and r_{AC} with z^s held fixed can be related to infinitesimal changes in x and y for fixed z^s using eq 8 and 9. Similarly an infinitesimal change in u^s at fixed z^s can be related to infinitesimal changes in x and y using eq 58 and 59. This allows a constant $-z^s$ version of eq 53 to be written

$$(dV)_{z^s} = {}^1/_2 F_{u^s}(s)[(du^s)_{z^s}]^2 \tag{61}$$

where

$$F_{u^s}(s) = \cos^2\theta(s)\{F^{AB} n_{AB}(s)[c_1 c_2^{-1} + \tan\theta(s)]^2 + F^{BC}[1 - n_{AB}(s)]c_2^{-2} + {}^1/_2 F^{AC} Bm(s)[1 + 4Bm(s)] \times [(1 - c_1)c_2^{-1} - \tan\theta(s)]\}^2 \tag{62}$$

Equations 29, 55, and 62 determine the necessary Morse parameters for the determination of the transverse vibrational energy levels using eq 24–26. The reactant vibrational energy levels are a special case of the above with $s = -\infty$ or $n_{AB}(s) = 0$. Notice that for the procedure in the literature,[1,16] as the transition state tends to the reactant or product configuration, the transverse vibrational frequency does not tend to the reactant or product vibrational frequency. The present procedure involves a more consistent treatment of the effective reduced mass for the transverse vibrational degree of freedom, and so it does satisfy these limits. It reduces exactly to Johnston and Parr's method[1,16] only for symmetric configurations (A = C and $r_{AB} = r_{BC}$); otherwise it generally predicts a higher $\omega_e(s)$.

Using assumption (2), the harmonic and anharmonic bending force constants of eq 30 are obtained from the repulsive AC interaction term as follows:

$$F_\Phi(s) = \left.\frac{d^2 V_{AM}^{AC}}{d\Phi^2}\right|_{r_{AB}=r_{AB}(s), r_{BC}=r_{BC}(s), \Phi=\pi} \tag{63}$$

$$= \frac{dV_{AM}^{AC}}{dr_{AC}}\left(\frac{\partial^2 r_{AC}}{\partial\Phi^2}\right)_{r_{AB}, r_{AC}}\Bigg|_{r_{AB}=r_{AB}(s), r_{BC}=r_{BC}(s), \Phi=\pi} \tag{64}$$

$$= a_M^{AC} D_e^{AC} Bm(s) q(s)[1 + 2Bm(s)] \tag{65}$$

and

$$A_\Phi(s) = {}^1/_2 F^{AC} Bm(s) q(s)\{3[1 + 4Bm(s)]q(s) - (A_M^{AC})^{-1}[1 + 2Bm(s)][1 - 3q(s)/r_{AC}(s)]\} \tag{66}$$

where we have defined

$$q(s) = \frac{r_{AB}(s) r_{BC}(s)}{r_{AC}(s)} \tag{67}$$

To calculate the imaginary frequency along the reaction coordinate requires the negative force constant of eq 40. For this we get

$$F_s(s=0) = \left(\frac{d^2V}{dn_{AB}(s)^2}\right)\Bigg|_{n_{AB}=n_{AB}^{\ddagger}} \left(\frac{\partial n_{AB}(s)}{\partial z^s}\right)_{u^s}^2\Bigg|_{s=0} \quad (68)$$

where $n_{AB}^{\ddagger}$ is $n_{AB}(s=0)$. The second derivative of V is easily evaluated analytically from eq 44, 47, 48, and 50-52. Finally eq 45, 46, 58, and 59 yield

$$\left(\frac{\partial n_{AB}(s)}{\partial z^s}\right)_{u^s}^2\Bigg|_{s=0} = \frac{1}{P^2}\frac{(1-n_{AB}^{\ddagger})^2(n_{AB}^{\ddagger})^2}{[1-n_{AB}^{\ddagger}(1+c_1)]^2+(c_2 n_{AB}^{\ddagger})^2} \quad (69)$$

Loose Transition States. It is interesting to examine the limit of the generalized transition-state theory rate as approximated by 12-18 and 24-37 in the limit of large internuclear separations, i.e., when $|s|$ becomes large. In eq 12 and 13, $Q_{str}^{GT}(T,s)$ and the Boltzmann factor tend to finite limits, but we next show that $Q_r^{GT}(T,s)$ and $Q_b^{GT}(T,s)$ diverge except at 0 K. Consider first the moment of inertia of eq 18

$$I(s) \underset{r_{XY}\to\infty}{\sim} C_{XY} r_{XY}^2 \quad XY = AB \text{ or } BC \quad (70)$$

where C_{XY} is constant. As the moment of inertia becomes large, the rotational partition function can be treated classically and

$$Q_r^{GT}(T,s) \underset{r_{XY}\to\infty}{\sim} (2k_B T C_{XY}/\hbar^2) r_{XY}^2 \quad (71)$$

Next consider the effective mass for bending defined by eq 31 and 32

$$m_\Phi(s) \underset{r_{AB}\to\infty}{\sim} m_{BC} r_{BC}^2 \quad (72)$$

$$m_\Phi(s) \underset{r_{BC}\to\infty}{\sim} m_{AB} r_{AB}^2 \quad (73)$$

But the bending force constants and thus the bending energy levels tend to zero exponentially. Thus the bending partition function diverges exponentially except at 0 K. Since canonical variational theory locates the dividing surface to minimize the rate, these divergences will prevent the dividing surface from being located too far into the reactant or product valley.

The source of the divergences is that it becomes unrealistic to apply eq 13 in the asymptotic region. In reality, as $|s|$ increases, the bends become first hindered rotations and then free rotations. A more accurate version of generalized transition-state theory in cases where the best dividing surface should occur at large $|s|$ where the bends are already appreciably free would be to consider the adiabatic correlation of A, BC orbital motions and BC rotations with ABC bends and ABC rotations,[35,36] and then to use microcanonical variational theory with these adiabatic potential curves.

If the intrinsic potential energy barrier occurs at such a large atom-diatom separation that the bending vibration has become free, it is probably negligibly small. Then it is customary to abandon the conventional transition-state framework with the dividing surface at the barrier and to calculate instead the rate of passage over the barrier in the effective potential, which is the sum of the centrifugal potential and the long-range attractive potential. For the reactants of an exoergic or thermoneutral reaction, the effective potential is

$$V_{eff}(R_{A,BC}, r_{BC}=r_e^{BC}) = \frac{\hbar^2 l(l+1)}{2\mu {R_{A,BC}}^2} - \frac{{C_6}^{A,BC}}{{R_{A,BC}}^6} \quad (74)$$

where l is the orbital angular momentum for motion of A relative to BC, $R_{A,BC}$ is the distance from A to the center of mass of BC, and ${C_6}^{A,BC}$ is due to dispersion and induction forces:

$${C_6}^{A,BC} = {C_{disp}}^{A,BC} + {C_{ind}}^{A,BC} \quad (75)$$

The dispersion term is approximated by the Slater-Kirkwood expression[37]

$${C_{disp}}^{A,BC} = \frac{3}{2}\frac{e^2\hbar^2}{m_e}\frac{\alpha_A\alpha_{BC}}{\left(\frac{\alpha_A}{N_A}\right)^{1/2}+\left(\frac{\alpha_{BC}}{N_{BC}}\right)^{1/2}} \quad (76)$$

where e and m_e are charge and mass of an electron and α_X and N_X are the polarizability and number of valence electrons of X; the induction term is given by[38]

$${C_{ind}} = {d_{BC}}^2\alpha_A \quad (77)$$

where d_{BC} is the dipole moment of BC.[39] The centrifugal barrier becomes higher and occurs closer in as l increases; the centrifugal barrier of height E_b occurs at

$${R_{A,BC}}^G(E_b) = (2{C_6}^{A,BC}/E_b)^{1/6} \quad (78)$$

Treating l classically and including contributions from all impact parameters such that the centrifugal barrier height is less than the relative translational energy E_{rel} yields the following rate constant for passage over the barrier:[1,27,40]

$$k^G(T) = \sqrt{\frac{\pi}{\mu}}\, 2^{11/6}\Gamma\left(\frac{2}{3}\right)({C_6}^{A,BC})^{1/3}(k_B T)^{1/6} \quad (79)$$

This expression was first derived by Gorin[40] and this will be called the Gorin model. When the Gorin rate is less than the conventional transition-state theory rate at a given temperature we use the Gorin rate instead. Of course the Gorin model should only be used if eq 74 is still valid at the distance ${R_{A,BC}}^{CB}(E_b)$ for the barrier heights of interest. The crucial barrier height for any given relative translational energy E_{rel} is the one with $E_b = E_{rel}$. It is easily shown that in the Gorin model the average value of E_{rel} for reacting systems is $1\frac{2}{3}k_B T$. Thus a condition for applicability of the Gorin model is that eq 74 be approximately correct at ${R_{A,BC}}^G(E_b = 1\frac{2}{3}k_B T)$. One approximate way to judge this is to use the BEBO method to compute the first-order contribution to the potential energy at this distance to see if that contribution is much smaller than the second-order attractive contribution in eq 74 and much smaller than $k_B T$.

Calculational Details

The variational calculation was carried out using the free-energy formulation, eq 12-20. The free-energy change, $\Delta G^{GT,0}(T,s)$, was computed for 19 values of the bond order $n_{AB}(s)$ from 0.05 to 0.95. The maximum was located and the 0.10 increment of bond order bracketing the maximum was subdivided into 0.005 bond-order increments. The free-energy change was calculated on the subdivided grid to locate a new maximum. The subdivision was repeated two more times for a final subdivision in bond order of 0.000 05. This allowed evaluation of the CVT rate constant to four significant figures.

Activation energies $E_a(T)$ are calculated as an average appropriate for the fixed temperature range 300-1000 K by

$$E_a(T) = k_B\frac{T_1 T_2}{T_2 - T_1}\ln[k(T_2)/k(T_1)] \quad (80)$$

where $T_1 = 300$ K and $T_2 = 1000$ K.

In order to test the quantitative adequacy of the procedures used here and elsewhere, we made a number of checks. These are summarized for eight representative cases in Table I. With two exceptions,[20,21] all previous calculations using the BEBO method have used harmonic vibrational potentials and classical rotational partition functions. First we checked the treatment of the bending potential. Define $\Phi_{CVTtp}(T)$ as the classical turning point of the potential of eq 30 for $s = s_*^{CVT}(T)$ with an energy of $k_B T$ in a bending degree of freedom. Table I compares the bending potential energy ΔV_b at this point using the full repulsive interaction ${V_{AM}}^{AC}(\Phi)$ of eq 49, using the

Table I. Tests of Procedures for Computing Partition Functions and Partition Function Ratios in Canonical Variational Theory at 600 K

reaction	$\Phi_{CVTtp}(T)$, deg	ΔV_b, kcal/mol			$[Q_b^{CVT}(harm)/Q_b^{CVT}(quart)]$	$\frac{[Q_{str}^{CVT}(harm)\cdot Q_{str}^{BC}(Morse)]}{[Q_{str}^{CVT}(Morse)\cdot Q_{str}^{BC}(harm)]}$	$\frac{[Q_r^{CVT}(class)\cdot Q_r^{BC}(quant)]}{[Q_r^{CVT}(quant)\cdot Q_r^{BC}(class)]}$
		V_{AM}^{AC}	$A_\Phi \neq 0$	$A_\Phi = 0$			
C + H_2	149	1.196	1.192	1.116	1.14	0.991	1.010
O + H_2	144	1.201	1.192	1.074	1.20	0.996	1.013
F + H_2	140	1.204	1.192	1.054	1.23	0.982	1.015
Li + HO	147	1.198	1.192	1.098	1.13	1.027	1.015
Li + HI	145	1.203	1.192	1.070	1.16	1.011	1.005
C + HC	150	1.198	1.192	1.097	1.15	1.009	1.012
O + HO	135	1.238	1.192	0.956	1.34	1.008	1.015
O + HCl	133	1.263	1.192	0.908	1.40	0.998	1.008
F + HCl	130	1.268	1.192	0.898	1.41	0.999	1.008
Br + HI	128	1.289	1.192	0.870	1.44	1.000	1.005

Table II. Comparison of Gorin Model to Conventional and Canonical Variational Transition State Theory Results for Seven Exothermic and Thermoneutral Reactions at 600 K

reaction A + BC	at saddle point			at CVT transition state			at $R_{A,BC}^G(E_b = \frac{5}{3}k_BT)^a$			$k^G(T)/k^{\ddagger}(T)$	$k^G(T)/k^{CVT}(T)$	$k^{\ddagger}(T)/k^{CVT}(T)$
	$R_{A,BC}$, a_0	V,[b] kcal/mol	$\Phi_{\ddagger tp}$, deg	$R_{A,BC}$, a_0	V,[b] kcal/mol	Φ_{CVTtp}, deg	$R_{A,BC}$, a_0	V,[b] kcal/mol	Φ_{Gtp}, deg			
O + HBr	6.87	0.126	97	5.94	−0.409	123	6.02	−0.276	119	7.23	17.43	2.41
F + HBr	7.29	0.073	85	6.16	−0.503	118	5.74	−1.984	128	3.91	11.05	2.83
F + HI	8.27	0.028	42	6.78	−0.587	110	5.87	−6.859	132	1.91	7.16	3.75
Cl + HBr	10.44	0.001	57	7.00	−0.888	113	6.92	−1.028	114	0.29	5.93	20.72
Br + HBr	8.31	0.119	100	6.89	−0.633	135	7.22	−0.152	114	6.21	19.92	3.21
Br + HI	8.87	0.136	101	7.63	−0.414	128	7.40	−0.864	132	6.33	15.44	2.44
I + HI	10.17	0.041	71	8.15	−0.678	123	7.63	−1.753	132	2.12	8.47	4.00

[a] $\frac{5}{3}k_BT$ is 1.987 kcal/mol at 600 K. [b] Potential energy computed from BEBO model.

mixed harmonic-quartic potential of eq 30, and using the harmonic approximation to the latter obtained by setting $A_\Phi = 0$. In most cases we find that the mixed harmonic-quartic potential is an excellent approximation, but the error in using a harmonic potential would be several times larger. Use of partition functions evaluated in the harmonic approximation rather than in the mixed harmonic-quartic approximation causes errors of 13–44% in the calculated rates at 600 K for the cases in Table I. This is comparable to the error caused in conventional transition-state theory by the comparable approximation.[20,21] The last two columns of the table show that the errors in using the harmonic approximation for stretches and the classical approximation for rotations are smaller. For large bending vibrational amplitudes, coupling with the rotational and stretching degrees of freedom becomes important. Although we have neglected such couplings in this study, they could be included in canonical variational calculations if desired. The coupling of the rotational and bending degrees of freedom has been studied in detail for conventional transition-state theory elsewhere.[21]

Results and Discussion

First we tested whether or not the Gorin model provides a variationally better transition state than a dividing surface through the saddle point. This would be possible only for a reaction with a very small intrinsic barrier height. Table II compares the models to one another and to canonical variational theory for all the reactions studied which have intrinsic barrier heights less than 0.2 kcal/mol. The table includes rate constant ratios and also the value of $R_{A,BC}$, the potential energy, and the bending turning point at the saddle point, at the canonical variational transition state, and at the centrifugal barrier when the centrifugal barrier height is $1\frac{2}{3}k_BT$. In each case, the bending turning point $\Phi_{\ddagger tp}$, Φ_{CVTtp}, or Φ_{Gtp} is computed for a bending vibrational energy of kT per bending degree of freedom. For all the reactions studied for temperatures up to 2400 K, the Gorin model predicts a smaller rate constant than conventional transition-state theory in only one case, Cl + HBr. In this case $k^{\ddagger}(T)/k^G(T) = 2.1$ at 300 K but $k^{CVT}(T)/k^G(T) = 0.14$. Thus even when the intrinsic barrier is very small there may be an entropic bottleneck at closer approach than the position of the centrifugal barrier for typical translational energies. In these cases canonical variational theory is more appropriate for calculating the rate than the Gorin model is. Notice also that, on the minimum energy path at $R_{A,BC} = R_{A,BC}^G(E_b = 1\frac{2}{3}kT)$, the BEBO method still predicts the existence of a turning point for the bending motion. In fact the values of $(\Phi - \pi)$ at the bending turning point for this position along the reaction path are still reasonably small. This is inconsistent with the assumptions of the Gorin model. It is also inconsistent with the Gorin model when the BEBO method predicts an appreciable first-order energy contribution at this distance. We conclude that canonical variational theory is much more appropriate for this kind of reaction with small intrinsic barriers than either the Gorin model or conventional transition-state theory.

Tables III–V present a set of rate constants and activation energies for all possible reactions A + BC → AB + C in which B is H and the BEBO input parameters correspond to A or C being H, Li, C, O, F, Cl, Br, or I. This set consists of 8 thermoneutral reactions and 28 nonthermoneutral reactions and their reverse reactions. We repeat that the BEBO method does not provide quantitatively reliable potential energy surfaces for these reactions and in some cases even the qualitative features may be different from those for the real system. For example, BEBO predicts a 6 kcal/mol symmetric barrier for F + HF and a shallow potential well for symmetric ClHCl flanked by twin 0.3 kcal/mol barriers,[41] but F + HF apparently really has a much higher barrier[42] and Cl + HCl may have a symmetric barrier of about 5 kcal/mol.[43] In addition BEBO predicts a larger effect of varying the dividing surface for the collinear H + H_2 reactions than is predicted[12] by calculations on that collinear reaction using a more accurate[44]

Table III. Rate Constants $k^{CVT}(T)$ (cm^3 molecule^{-1} s^{-1}), Ratios $k^{\ddagger}(T)/k^{CVT}(T)$, and Tunneling Correction Factors $\kappa^{W}(T)$ for the Reactions A + HC → AH + C at 300 K

	C							
A	H[a]	Li	C	O	F	Cl	Br	I
H	1.28×10^{-17} [b]	2.79×10^{-15}	4.24×10^{-20}	4.80×10^{-20}	3.79×10^{-36}	1.43×10^{-15}	1.52×10^{-13}	2.42×10^{-12}
	1.95[c]	1.11	7.94	1.90	1.08	1.45	1.11	1.26
	3.95[d]	1.36	3.94	1.98	1.14	2.01	1.25	1.10
Li	2.72×10^{-50}	2.03×10^{-26}	2.78×10^{-61}	3.92×10^{-55}	1.53×10^{-76}	7.42×10^{-55}	1.52×10^{-41}	2.51×10^{-24}
	1.11	1.82	1.03	1.19	1.15	1.10	1.11	1.48
	1.36	5.64	1.41	1.05	1.09	1.07	1.04	1.00
C	5.79×10^{-21}	3.89×10^{-27}	7.48×10^{-21}	7.66×10^{-23}	7.17×10^{-39}	2.17×10^{-18}	6.91×10^{-15}	4.37×10^{-13}
	7.94	1.03	24.7	1.21	1.16	1.43	1.06	1.17
	3.94	1.41	3.83	1.57	1.06	1.54	1.05	1.01
O	3.54×10^{-15}	2.97×10^{-15}	4.14×10^{-17}	9.93×10^{-15}	2.58×10^{-30}	3.49×10^{-12}	1.26×10^{-11}	8.57×10^{-12}
	1.90	1.19	1.21	312	1.54	1.63	2.03	1.68
	1.98	1.05	1.57	2.08	1.01	1.00	1.00	1.00
F	6.14×10^{-13}	2.54×10^{-18}	8.51×10^{-15}	5.67×10^{-12}	7.62×10^{-16}	6.19×10^{-12}	1.88×10^{-11}	3.27×10^{-11}
	1.08	1.15	1.16	1.54	640	1.67	2.33	3.00
	1.14	1.09	1.06	1.01	2.48	1.00	1.00	1.00
Cl	9.57×10^{-16}	5.09×10^{-20}	1.06×10^{-17}	3.17×10^{-17}	2.56×10^{-35}	5.48×10^{-12}	5.60×10^{-11}	1.06×10^{-11}
	1.45	1.10	1.43	1.63	1.67	2.18	7.77[e]	1.73
	2.01	1.07	1.54	1.00	1.00	1.00	1.00	1.00
Br	7.42×10^{-25}	7.60×10^{-18}	2.74×10^{-25}	8.39×10^{-28}	5.67×10^{-46}	4.08×10^{-22}	1.04×10^{-11}	1.18×10^{-11}
	1.11	1.11	1.06	2.03	2.33	7.77[e]	2.43	1.98
	1.25	1.04	1.05	1.00	1.00	1.00	1.00	1.00
I	2.74×10^{-35}	2.92×10^{-12}	3.64×10^{-35}	1.32×10^{-39}	2.29×10^{-57}	1.80×10^{-34}	2.72×10^{-23}	2.46×10^{-11}
	1.26	1.48	1.17	1.68	3.00	1.73	1.98	3.02
	1.10	1.00	1.01	1.00	1.00	1.00	1.00	1.00

[a] Results for this column include reaction with both ends. [b] Top entry is rate constant $k^{CVT}(T)$ of canonical variational theory with unit transmission coefficient. [c] Middle entry is ratio $k^{\ddagger}(T)/k^{CVT}(T)$ of conventional transition-state theory rate constant to canonical variational theory one. [d] Bottom entry is Wigner tunneling correction factor $\kappa^{W}(T)$. [e] When the Gorin rate constant is smaller than the conventional transition-state theory one for an exoergic or thermoneutral reaction it is used instead, and the rate constant for the endothermic reaction is calculated using the Gorin exoergic rate constant and detailed balance. The only case where this occurred is Cl + HBr.

Table IV. Rate Constants $k^{CVT}(T)$ (cm^3 molecule^{-1} s^{-1}), Ratios $k^{\ddagger}(T)/k^{CVT}(T)$, and Tunneling Correction Factors $\kappa^{W}(T)$ for the Reactions A + HC → AH + C at 1000 K

	C							
A	H[a]	Li	C	O	F	Cl	Br	I
H	1.32×10^{-12} [b]	4.07×10^{-12}	9.51×10^{-14}	1.23×10^{-13}	2.35×10^{-18}	2.49×10^{-12}	1.30×10^{-11}	4.23×10^{-11}
	1.19[c]	1.17	1.99	1.15	1.18	1.06	1.21	1.48
	1.27[d]	1.03	1.26	1.09	1.01	1.09	1.02	1.01
Li	5.86×10^{-22}	2.03×10^{-15}	4.33×10^{-26}	6.68×10^{-24}	1.91×10^{-30}	4.01×10^{-24}	4.31×10^{-20}	8.02×10^{-15}
	1.17	1.91	1.04	1.25	1.17	1.13	1.16	2.51
	1.03	1.42	1.04	1.00	1.01	1.01	1.04	1.00
C	1.20×10^{-13}	3.79×10^{-16}	4.19×10^{-14}	1.13×10^{-14}	2.03×10^{-19}	1.81×10^{-13}	2.46×10^{-12}	6.19×10^{-11}
	1.99	1.04	4.10	1.04	1.20	1.09	1.12	1.33
	1.26	1.04	1.25	1.05	1.01	1.05	1.00	1.00
O	6.66×10^{-12}	2.52×10^{-12}	4.86×10^{-13}	3.67×10^{-12}	1.14×10^{-16}	2.24×10^{-11}	4.73×10^{-11}	4.01×10^{-11}
	1.15	1.25	1.04	8.39	1.93	2.00	2.80	2.23
	1.09	1.00	1.05	1.10	1.00	1.00	1.00	1.00
F	3.80×10^{-11}	2.15×10^{-13}	2.60×10^{-12}	3.40×10^{-11}	1.44×10^{-12}	3.27×10^{-11}	6.01×10^{-11}	8.79×10^{-11}
	1.18	1.17	1.20	1.93	10.4	2.18	3.34	4.50
	1.01	1.01	1.01	1.00	1.13	1.00	1.00	1.00
Cl	6.14×10^{-12}	6.87×10^{-14}	3.53×10^{-13}	1.02×10^{-12}	4.98×10^{-18}	2.16×10^{-11}	1.06×10^{-10}	4.42×10^{-11}
	1.06	1.13	1.09	2.00	2.18	3.70	5.02[e]	2.44
	1.09	1.01	1.05	1.00	1.00	1.00	1.00	1.00
Br	1.71×10^{-14}	3.95×10^{-13}	2.58×10^{-15}	1.15×10^{-15}	4.91×10^{-21}	5.68×10^{-14}	3.10×10^{-11}	4.10×10^{-11}
	1.21	1.16	1.12	2.80	3.34	5.02[e]	4.16	2.93
	1.02	1.04	1.00	1.00	1.00	1.00	1.00	1.00
I	2.18×10^{-17}	2.88×10^{-11}	4.89×10^{-18}	3.81×10^{-19}	2.81×10^{-24}	9.26×10^{-18}	1.60×10^{-14}	6.14×10^{-11}
	1.48	2.51	1.33	2.23	4.50	2.44	2.93	5.10
	1.01	1.00	1.00	1.00	1.00	1.00	1.00	1.00

[a] Results for this column include reaction with both ends. [b] Top entry is rate constant $k^{CVT}(T)$ of canonical variational theory with unit transmission coefficient. [c] Middle entry is ratio $k^{\ddagger}(T)/k^{CVT}(T)$ of conventional transition-state theory rate constant to canonical variational theory one. [d] Bottom entry is Wigner tunneling correction factor $\kappa^{W}(T)$. [e] When the Gorin rate constant is smaller than the conventional transition-state theory one for an exoergic or thermoneutral reaction it is used instead, and the rate constant for the endothermic reaction is calculated using the Gorin exoergic rate constant and detailed balance. The only case where this occurred is Cl + HBr.

potential surface. In contrast, the BEBO predictions for the effect of varying the surface location for the collinear Cl + H_2 reaction are in qualitative agreement with predictions[12] based on a semiempirical extended LEPS potential surface.[45] In most cases there is not enough information to judge the accuracy of the BEBO potential surface. For the present study we use

Table V. Activation Energies E_a^{CVT} and Differences $E_a^{\ddagger} - E_a^{CVT}$ and $E_a^{CVT/W} - E_a^{CVT}$ for the Reactions A + HC → AH + C for the Temperature Range 300-1000 K[a]

	C							
A	H	Li	C	O	F	Cl	Br	I
H	9.83[b]	6.20	12.45	12.57	34.89	6.36	3.79	2.44
	−0.42[c]	0.04	−1.18	−0.43	0.08	−0.27	0.08	0.14
	−0.97[d]	−0.23	−0.98	−0.51	−0.10	−0.52	−0.17	−0.07
Li	55.56	21.57	69.01	62.24	90.40	60.27	42.07	18.64
	0.04	0.04	0.003	0.04	0.02	0.02	0.03	0.45
	−0.23	−1.18	−0.26	−0.04	−0.07	−0.05	−0.03	−0.003
C	14.35	21.55	13.23	16.02	38.14	9.65	5.00	2.82
	−1.18	0.003	−1.53	−0.13	0.03	−0.23	0.04	0.11
	−0.97	−0.26	−0.95	−0.03	−0.04	−0.33	−0.04	−0.01
O	6.42	5.74	7.98	5.04	26.76	1.58	1.12	1.31
	−0.43	0.04	−0.13	−3.08	0.19	0.17	0.27	0.24
	−0.51	−0.04	−0.03	−0.55	−0.005	−0.004	−0.001	−0.001
F	3.51	9.66	4.87	1.53	6.43	1.42	0.99	0.84
	0.08	0.02	0.03	0.19	−3.51	0.22	0.31	0.34
	−0.10	−0.07	−0.04	−0.005	−0.67	−0.002	0.0	0.0
Cl	7.47	12.02	8.87	8.84	33.90	1.17	0.54	1.22
	−0.27	0.02	−0.23	0.17	0.22	0.45	−0.37[e]	0.29
	−0.52	−0.05	−0.33	−0.004	−0.002	−0.001	0.0	0.0
Br	20.32	9.25	19.65	23.80	48.90	15.97	0.93	1.07
	0.08	0.03	0.04	0.27	0.31	−0.37[e]	0.46	0.34
	−0.17	−0.03	−0.04	−0.001	0.0	0	0.0	0.0
I	35.11	1.95	33.59	40.13	64.89	32.77	17.20	0.78
	0.14	0.45	0.11	0.24	0.34	0.29	0.34	0.45
	−0.07	−0.003	−0.01	−0.001	0.0	0.0	0.0	0.0

[a] Computed from results in Tables IV and V. [b] Top entry is activation energy computed by canonical variational theory with unit transmission coefficient. [c] Middle entry is difference of conventional transition-state theory activation energy from canonical variational theory one. [d] Bottom entry is difference of activation energy computed with Wigner tunneling correction factor from one computed without it. [e] For Cl + HBr, Gorin model is substituted for conventional transition-state theory.

Table VI. Median Value $k^{\ddagger}(T)/k^{CVT}(T)$ for the Reactions A + HC → AH + C as a Function of Temperature

T, K	median overestimate factor in conventional theory
200	1.60
300	1.65
600	1.75
1000	1.92
2400	2.01

the surfaces obtained using the parameters for all combinations of the eight A's and eight B's in order to generate a sample of test cases to learn about the general effects of varying the dividing surfaces on the calculated rates. For this purpose it is not necessary that the potential surfaces studied quantitatively represent real systems. Thus it is not our goal to compare to experiment for the systems nominally represented. We also emphasize that even the 36 cases studied do not include representatives of every possible kind of potential surface topology. For example, none of the 36 cases is very similar to the semiempirical valence-bond surface of Raff et al.[46] for H + HI. The Raff et al. surface has an intrinsic barrier height of 0.06 kcal/mol at a H-H distance of $2.42a_0$ (compared to $r_e^{HH} = 1.40a_0$) whereas the BEBO surface for H + HI has a 1.07 kcal/mol intrinsic barrier at $3.27a_0$. The earlier barrier on the BEBO surface means that there is much less change in the transverse vibrational well by the time the barrier is reached than for the Raff et al. surface. It is not known which of the two predicted barrier positions is more correct for H + HI, but the BEBO surface still provides an interesting test case that is representative of one kind of potential surface that may occur in general in some real system.

Examination of the tables shows that in most cases there is a large effect of variationally optimizing the location of the dividing surface. The average value $k^{\ddagger}(T)/k^{CVT}(T)$ for the 36 reactions is 20 at 300 K and 2.5 at 1000 K. However, since a few values of this ratio are quite large, the median value is much more meaningful than the mean. The median is given as a function of temperature in Table VI. Notice that, although the median value of the ratio increases with temperature, the ratio itself may either increase or decrease with temperature.

Table VII presents further details of the conventional transition state and the 600 K canonical variational one which help us to better understand the origin of the effect of moving the dividing surface on the calculated rate constant and the origin of the temperature dependence of $k^{\ddagger}(T)/k^{CVT}(T)$. All four factors which contribute to $k^{\ddagger}(T)/k^{CVT}(T)$ are given; these are the ratios of generalized transition-state partition functions for bending, rotation, and transverse stretching and the ratio of classical Boltzmann factors at the bottom of the transverse vibrational well for the two locations of the dividing surface. The last factor is always less than unity, i.e., it always favors locating the dividing surface at the saddle point. However, at least one of the other factors, and usually three, favors moving the dividing surface to another location. In general, at least one of the vibrational degrees of freedom is more important in determining the location of the generalized transition state than the rotational degree of freedom. This is because the rotational energy levels are much more closely spaced than the vibrational ones and the rotational partition function is given to a good approximation by the classical expression which is directly proportional to the moment of inertia:

$$Q_{rot}^{GT}(T,s) \simeq 2I(s)k_BT/\hbar^2 \qquad (81a)$$

Therefore the ratio of the rotational partition function at the saddle point to that at the CVT generalized transition state is approximately given by $I(s = 0)/I[s = s_*^{CVT}(T)]$. The vibrational degrees of freedom behave more quantum mechanically, and the variation in the energy levels $\epsilon_{str,n}^{GT}(s)$ and $\epsilon_{b,n}^{GT}(s)$ as functions of location along the reaction coordinate enters the partition function ratio through exponentials. Thus

Table VII. Detailed Quantities Characterizing the Various Reactions and Ratios of Conventional Transition-State Theory to Canonical Variational Theory Ones at Three Temperatures

					T = 600 K									T = 200 K	T = 2400 K
reaction A + BC ↔ AB + C	β,[a] deg	ΔV,[b] kcal/mol	$V_{MEP}(s=0)$,[c] kcal/mol	$n_{AB}^{\ddagger}$[d]	$\Phi_{\ddagger tp}$,[e] deg	$\kappa^{W}(T)$[f]	$n_{AB}(s_*^{CVT})$[g]	Φ_{CVTtp},[h] deg	$Q^{\ddagger}(T)/Q^{CVT}$ bends[i]	rotation[j]	stretch[k]	$e^{\Delta V^{CVT}}(T)/k_BT$[l]	$k^{\ddagger}(T)/k^{CVT}(T)$	$k^{\ddagger}(T)/k^{CVT}(T)$	$k^{\ddagger}(T)/k^{CVT}(T)$
H + H_2 ↔ H_2 + H	60.0	0.0	9.9	0.50	146	1.74	0.35	146	0.93	0.97	2.44	0.61	1.36	2.78	1.14
Li + H_2 ↔ LiH + H	48.6	53.4	4.4	0.94	144	1.09	0.91	145	1.17	1.04	1.03	0.91	1.13	1.12	1.28
C + H_2 ↔ CH + H	47.2	3.9	10.7	0.55	150	1.73	0.40	149	1.04	0.96	4.93	0.57	2.84	22.69	1.68
O + H_2 ↔ OH + H	46.7	−5.3	5.5	0.38	145	1.24	0.30	144	0.94	0.95	1.68	0.88	1.32	2.72	1.05
F + H_2 ↔ FH + H	46.4	−31.1	1.9	0.09	137	1.04	0.12	140	1.19	1.09	0.94	0.92	1.12	1.07	1.33
Cl + H_2 ↔ ClH + H	45.8	3.0	5.0	0.74	149	1.25	0.79	148	0.88	0.98	1.38	0.95	1.15	1.81	1.20
Br + H_2 ↔ BrH + H	45.4	18.9	2.2	0.93	142	1.06	0.89	144	1.25	1.05	0.97	0.91	1.15	1.10	1.35
I + H_2 ↔ IH + H	45.2	35.5	1.1	0.98	132	1.02	0.95	138	1.52	1.10	1.02	0.80	1.36	1.24	1.80
Li + HLi ↔ LiH + Li	29.0	0.0	20.9	0.50	148	2.16	0.41	148	0.99	1.00	2.56	0.71	1.78	2.09	2.21
C + HLi ↔ CH + Li	26.1	−49.5	19.2	0.18	160	1.10	0.19	160	1.03	1.01	1.01	0.97	1.03	1.04	1.06
O + HLi ↔ OH + Li	24.9	−58.7	4.0	0.05	145	1.01	0.08	147	1.19	1.07	1.11	0.85	1.20	1.22	1.43
F + HLi ↔ FH + Li	24.3	−84.5	7.6	0.06	153	1.02	0.08	154	1.13	1.05	1.09	0.88	1.14	1.18	1.31
Cl + HLi ↔ ClH + Li	22.8	−50.4	10.0	0.08	157	1.02	0.11	157	1.10	1.04	1.05	0.91	1.10	1.12	1.23
Br + HLi ↔ BrH + Li	21.7	−34.5	7.4	0.08	152	1.01	0.12	153	1.12	1.05	1.06	0.90	1.12	1.13	1.28
I + HLi ↔ IH + Li	21.3	−17.9	1.0	0.009	130	1.00	0.15	145	2.58	1.42	1.15	0.45	1.91	1.38	3.38
C + HC ↔ CH + C	22.7	0	12.7	0.50	151	1.71	0.37	150	0.96	0.99	10.06	0.64	6.12	116.2	3.49
O + HC ↔ OH + C	21.3	−9.2	6.3	0.36	149	1.14	0.32	149	0.96	0.99	1.17	0.97	1.08	1.36	1.01
F + HC ↔ FH + C	20.6	−35.0	3.0	0.11	146	1.01	0.15	148	1.20	1.06	1.04	0.88	1.17	1.18	1.32
Cl + HC ↔ ClH + C	18.7	−0.9	7.3	0.63	153	1.14	0.68	152	0.95	0.99	1.31	0.95	1.17	1.74	1.04
Br + HC ↔ BrH + C	17.4	15.0	3.4	0.87	147	1.01	0.84	148	1.13	1.03	1.00	0.94	1.09	1.06	1.20
I + HC ↔ IH + C	16.9	31.6	1.4	0.96	138	1.00	0.93	142	1.33	1.08	1.02	0.85	1.24	1.16	1.55
O + HO ↔ OH + O	19.8	0.0	4.3	0.50	137	1.27	0.67	135	0.92	0.97	31.16	0.75	20.73	5438.	4.99
F + HO ↔ FH + O	19.1	−25.8	0.3	0.04	111	1.00	0.10	127	1.91	1.22	1.00	0.74	1.73	1.48	2.38
Cl + HO ↔ ClH + O	17.0	8.3	0.3	0.96	119	1.00	0.86	133	1.99	1.20	1.06	0.71	1.81	1.59	2.41
Br + HO ↔ BrH + O	15.5	24.2	0.13	0.993	97	1.00	0.95	123	2.68	1.33	1.06	0.64	2.41	1.89	3.77
I + HO ↔ IH + O	15.0	40.8	0.2	0.994	110	1.00	0.97	128	2.18	1.25	1.05	0.68	1.94	1.58	2.96
F + HF ↔ FH + F	18.3	0.0	5.8	0.50	139	1.37	0.65	137	0.92	0.98	46.57	0.71	29.68	15 950	5.58
Cl + HF ↔ ClH + F	16.1	34.1	0.3	0.987	112	1.00	0.95	130	2.13	1.25	1.05	0.68	1.92	1.60	2.84
Br + HF ↔ BrH + F	14.5	50.0	0.07	0.997	85	1.00	0.97	118	3.13	1.39	1.05	0.62	2.82	2.13	4.64
I + HF ↔ IH + F	13.9	66.6	0.03	0.9992	61	1.00	0.983	110	4.04	1.49	1.05	0.60	3.75	2.69	6.42
Cl + HCl ↔ ClH + Cl	13.6	0.0	0.3	0.992	117	1.00	0.88	143	3.75	1.48	0.98	0.53	2.86	1.98	5.10
Br + HCl ↔ BrH + Cl	11.6	15.9	0.001	1.000	−57[m]	1.00	0.981	113	19.54	2.22	1.01	0.47	20.72	12.24	44.33
I + HCl ↔ IH + Cl	10.9	32.5	0.2	0.998	109	1.00	0.983	130	2.39	1.29	1.01	0.67	2.07	1.60	3.37
Br + HBr ↔ BrH + Br	9.1	0.0	0.12	0.998	100	1.00	0.95	135	4.04	1.50	1.00	0.53	3.21	2.15	6.81
I + HBr ↔ IH + Br	8.2	16.6	0.14	0.998	101	1.00	0.980	128	2.85	1.35	1.01	0.63	2.44	1.79	4.19
I + HI ↔ IH + I	7.2	0.0	0.04	0.9998	71	1.00	0.986	123	4.70	1.56	1.00	0.55	4.00	2.63	8.38

[a] Skew angle, i.e., angle between r_{AB} and r_{BC} axes in (x, y) plane. [b] Classical exoergicity for the forward reaction. [c] Intrinsic classical barrier height, i.e., classical barrier height in exoergic or thermoneutral direction. [d] AB bond order at conventional transition state. [e] Bond angle at turning point for bend at $s = 0$ with bending energy kT per degree of freedom at 600 K. [f] Wigner tunneling correction factor at 600 K. [g] AB bond order at canonical variational transition state at 600 K. [h] Bond angle at turning point for bend at canonical variational transition state at 600 K with bending energy kT per degree of freedom. [i] Square of the ratio of bending partition functions at 600 K. [j] Ratio of transition-state rotational partition functions at 600 K. [k] Ratio of transition-state stretching partition functions at 600 K. [l] $\exp[-[V_{MEP}(s=0) - V_{MEP}(s=s_*^{CVT})]/kT]$. [m] The mixed harmonic-quartic bending potential predicts an unphysical turning point angle less than zero for the Br + HCl reaction at the saddle point.

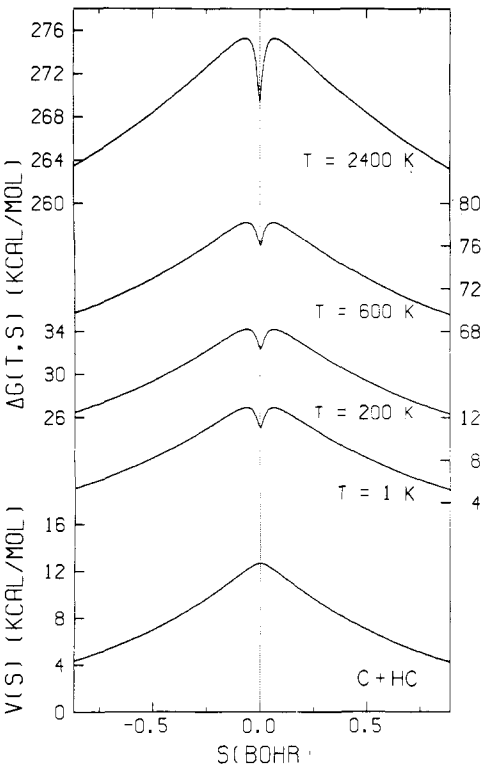

Figure 1. Classical potential energy barrier and generalized free energy of activation curves for the reaction C + HC → CH + H. The lowest curve is the potential energy barrier with the zero of energy taken at the bottom of the asymptotic reactant well. The generalized free energy of activation curves are given at temperatures of 1, 200, 600, and 2400 K for a standard state of 1 cm^3/molecule. The dotted line indicates the saddle point value of s, i.e., $s = 0$. For each of Figures 1-10, the reaction A + BC is thermoneutral or endothermic, and the range of reaction coordinate shown is from that corresponding to $n_{AB} = 0.05$ to $n_{AB} = 1 - 0.1n_{BC}^{\ddagger}$.

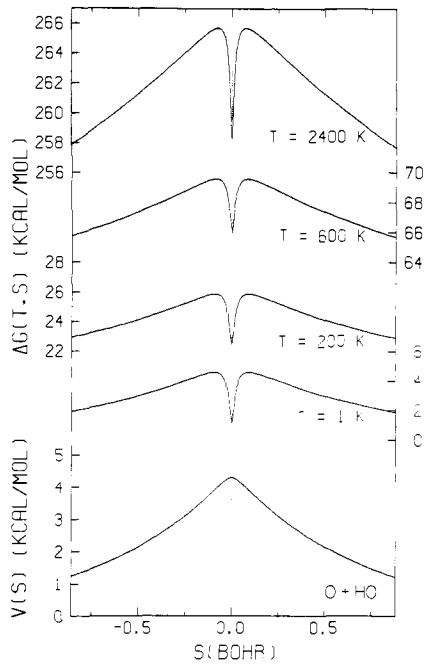

Figure 2. Same as Figure 1 except for the reaction O + HO → OH + O.

small changes in the vibrational energy levels can give large changes in the vibrational partition function, whereas comparable changes in the moment of inertia cause only small changes in the rotational partition functions.

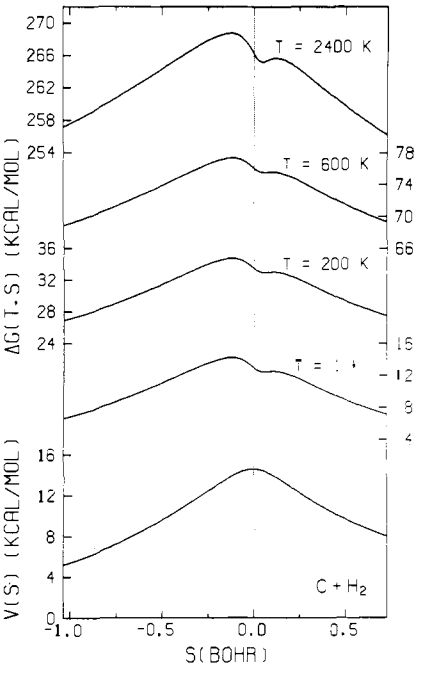

Figure 3. Same as Figure 1 except for the reaction C + H_2 → CH + H.

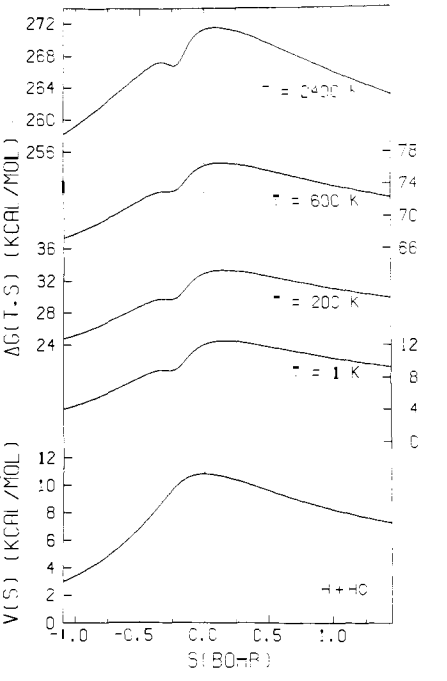

Figure 4. Same as Figure 1 except for the reaction H + HO → H_2 + O.

It is interesting to discuss these factors in more detail for several typical examples. For this purpose it will also be helpful to refer to Figures 1-10, which show the classical potential energy barrier and generalized free energy of activation curves for ten cases which are broadly representative of all the different kinds of results we found in this study. All ten figures show the generalized free energy of activation curves for temperatures of 1, 200, 600, and 2400 K. At sufficiently low temperatures contributions to the vibrational and rotational partition functions come only from the zero-point energies and it can be shown that

$$\Delta G^{GT,0}(T,s) \underset{T\to 0}{\sim} V_{MEP}(s) + \epsilon_{str,0}{}^{GT}(s) + 2\epsilon_{b,0}{}^{GT}(s) \epsilon_{str,0}{}^{BC}(s) - RT \ln \sigma \quad (81b)$$

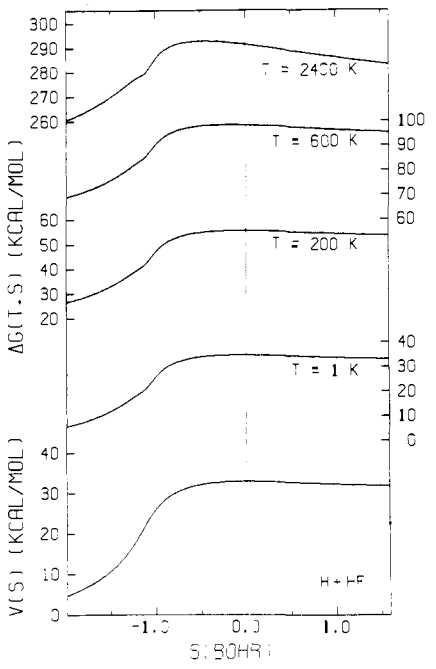

Figure 5. Same as Figure 1 except for the reaction H + HF → H_2 + F.

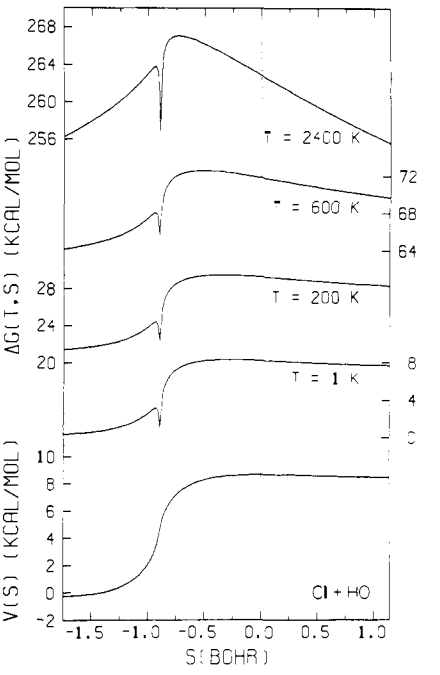

Figure 7. Same as Figure 1 except for the reaction Cl + HO → ClH + O.

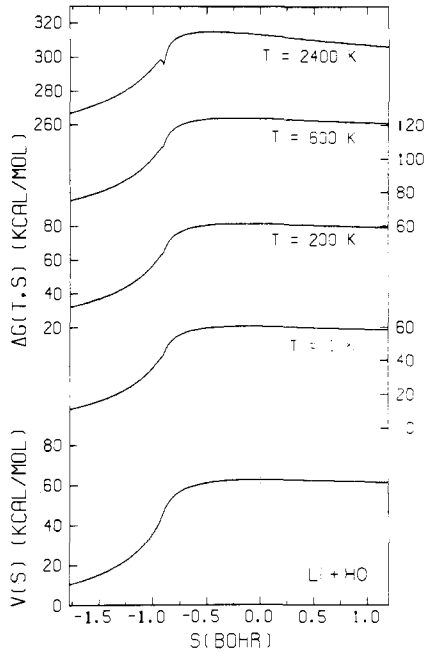

Figure 6. Same as Figure 1 except for the reaction Li + HO → LiH + O.

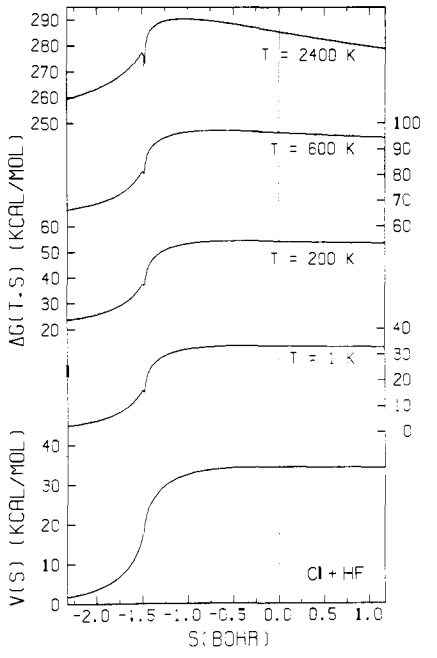

Figure 8. Same as Figure 1 except for the reaction Cl + HF → ClH + F.

since we have assumed $\kappa(T)$ to be unity in calculating $\Delta G^{GT,0}(T,s)$. When the symmetry factor σ is unity, the low-temperature limit of the generalized free energy of activation is just the adiabatic potential for the ground state with no angular momentum and with its zero taken at the zero-point level of the reactant. Comparing the generalized free energy of activation curve for $T = 1$ K to the potential barrier indicates how the vibrational zero-point energy levels for the stretching and bending motions change along the reaction coordinate. For higher temperatures higher energy levels of the vibrations become important, especially for the bending motion, and the rotational degree of freedom also makes contributions to the generalized free energy of activation. It is interesting to note that, although the magnitude of the generalized free energy of activation is a strong function of temperature, the overall qualitative shapes of the free-energy curves are similar for the different temperatures. In each figure $s = 0$ corresponds to the position of the conventional transition state, i.e., the saddle point. The sharp dips in several of the free-energy curves are due to the sharp dips in $\epsilon_{str,n}^{GT}(s)$ in the corner turning region; inspection of contour maps (not included in this paper) for realistic potential energy surfaces plotted in scaled and skewed coordinate systems confirms that the channel often widens appreciably in the region of large reaction path curvature.

Consider first the two symmetric reactions C + HC and O + HO. In all reactions with symmetrically situated saddle

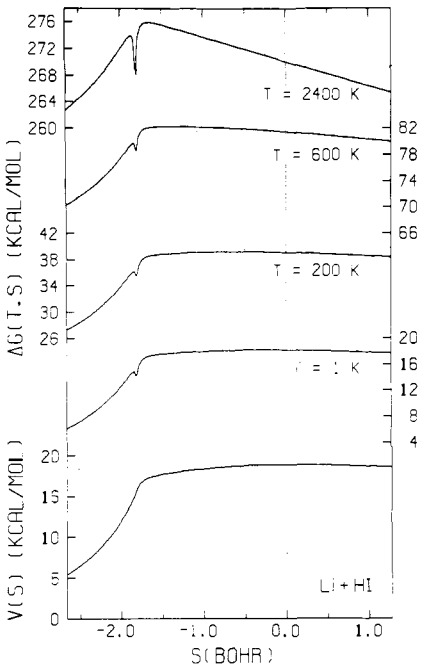

Figure 9. Same as Figure 1 except for the reaction Li + HI → LiH + I.

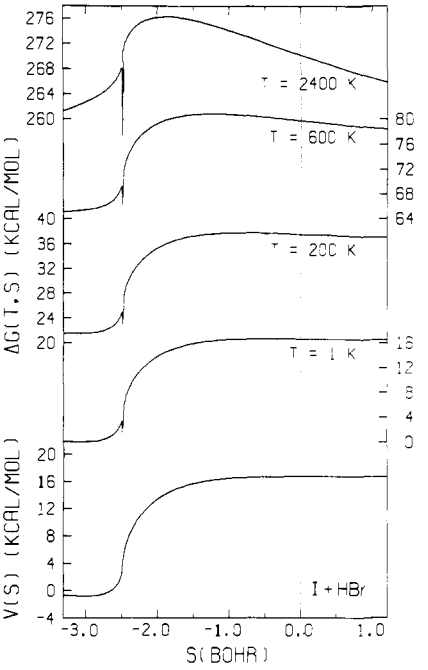

Figure 10. Same as Figure 1 except for the reaction I + HBr → IH + Br.

points the stretching degree of freedom was found to be the degree of freedom which most greatly influences $k^{\ddagger}(T)/k^{CVT}(T)$. Symmetric saddle points are located where the reaction coordinate turns the corner in going from reactants to products. In this corner, as mentioned in the last paragraph, the stretching vibrational potential widens considerably causing a drop in the vibrational energy levels. This causes the free-energy curves to have local minima at the saddle point locations for the C + HC and O + HO systems as seen in Figures 1 and 2. Therefore the stretching degree of freedom favors the CVT transition state to be located away from the saddle point for both these reactions. The harmonic frequency of the bending vibration is a local maximum at the saddle point; therefore, moving away from the saddle point lowers the bending vibrational energy levels. The moment of inertia is a local minimum at the saddle point so that the rotational energy levels also decrease as the generalized transition state is moved from the saddle point location. Thus both the bending vibrational and the rotational degrees of freedom favor location of the CVT transition state at the saddle point as seen by the partition function ratios less than unity in Table VII. However, both the bending vibrational frequency and the moment of inertia are slowly varying near the saddle point, and the competition between the classical potential energy barrier and the quantized stretching degree of freedom is the dominant factor in determining the location of the CVT transition state.

Although the C + HC and O + HO reactions have qualitatively similar free-energy curves, the O + HO reaction shows larger differences between the conventional and canonical variational transition-state theory results. In moving the generalized transition state from the saddle point to the CVT transition state at 600 K, the stretching vibrational frequency increases by 1730 cm^{-1} for the C + HC reaction and increases by 2710 cm^{-1} for the O + HO reaction. This much larger change in the zero-point energy for the O + HO reaction causes the ratio of rate constants $k^{\ddagger}(T)/k^{CVT}(T)$ to be much larger in this system than for C + HC. The frequency shift in moving the generalized transition state is much larger in the O + HO system than for C + HC for two reasons. First, the potential energy barrier is lower for O + HO, and the potential changes more slowly near the saddle point for this reaction than for C + HC. This energetic effect allows the CVT transition state to move further from the saddle point in the O + HO reaction, i.e., at $T = 600$ K, $s_*^{CVT} = -0.08a_0$ for O + HO and $-0.06a_0$ for C + HC. Second, the stretching frequency for the O + HO system is a more rapidly varying function of the distance along the reaction coordinate from the saddle point.

It is interesting to note that the ratio of rate constants $k^{\ddagger}(T)/k^{CVT}(T)$ decreases with increasing temperature for the two reactions C + HC and O + HO. Consider the C + HC reaction. The product of the bend and rotation partition function ratios is between 0.91 and unity for temperatures in the range 200–2400 K. Neglecting these two degrees of freedom the ratio of rate constants can be approximated in its low-temperature, quantal limit as

$$k^{\ddagger}(T)/k^{CVT}(T) \underset{T\to 0}{\sim} \exp\{[\tfrac{1}{2}\hbar\Delta\omega^{CVT}(T) + \Delta V^{CVT}(T)]/k_B T\} \quad (82)$$

where

$$\Delta\omega^{CVT}(T) = \omega_e[s = s_*^{CVT}(T)] - \omega_e(s = 0) \quad (83)$$

and

$$\Delta V^{CVT}(T) = V_{MEP}[s = s_*^{CVT}(T)] - V_{MEP}(s = 0) \quad (84)$$

Similarly in the high-temperature, classical limit

$$k^{\ddagger}(T)/k^{CVT}(T) \underset{T\to\infty}{\sim} \frac{\omega_e[s = s_*^{CVT}(T)]}{\omega_e(s = 0)} \times \exp[\Delta V^{CVT}(T)/k_B T] \quad (85)$$

For the C + HC reaction $\Delta\omega^{CVT}(T) > 0$ and for all systems $\Delta V^{CVT}(T) \leq 0$. For C + HC the variation $\hbar\Delta\omega^{CVT}(T)/2$ in the zero-point vibrational energy is greater than the magnitude $|\Delta V^{CVT}(T)|$ of the variational of the potential energy and thus eq 82 is a monotonically decreasing function of temperature. However, eq 85 monotonically increases with temperature for this system. This kind of behavior shows that is is possible to have the ratio $k^{\ddagger}(T)/k^{CVT}(T)$ go through a minimum as a function of temperature. Although no minimum is seen for either C + HC or O + HO in the 200–2400 K range studied, minima are observed in the reactions Cl + H_2, Li + HLi, C + HLi, O + HLi, F + HLi, Cl + HLi, Br + HLi, and F + HC.

For the C + HC system, it is interesting to compare the observed ratio $k^{\ddagger}(T)/k^{CVT}(T)$ with the high- and low-temperature limits, eq 82 and 85, respectively. The observed values of $k^{\ddagger}(T)/k^{CVT}(T)$ are 116.2, 6.12, and 3.49 at 200, 600, and 2400 K, respectively. The low-temperature limit gives 136, 5.1, and 1.5 for the same temperatures, while the high-temperature limit gives 0.97, 2.4, and 3.4 for the same temperatures.

The next eight systems are considered in order of increasingly "loose" transition states. The C + H_2 reaction has a nearly symmetrically located saddle point. Although $n_{AB}^{\ddagger}$ is greater than 0.5 for this system (see Table VII), the saddle point is located toward reactants, that is, it is located before the reaction coordinate turns the corner in going from reactants to products. The stretching vibrational frequency decreases in moving from the saddle point toward the corner. Because the saddle point is very near the corner the stretching vibrational frequency is rapidly varying. Although the maxima in the free-energy curves for temperatures of 200–2400 K are shifted only slightly from the saddle point [$s_*^{CVT}(T) \simeq -0.12a_0$ to $-0.13a_0$ for this temperature range], the stretching frequency increases by 1330–1420 cm^{-1}. The bending vibrational frequency increases by only 10–11 cm^{-1} for the same shift in location of the generalized transition state. The moment of inertia is also a slowly varying function of s; the ratio of the moment of inertia at the saddle point to that at $s_*^{CVT}(T)$ is 0.95–0.96 for $s_*^{CVT}(T) = -0.12a_0$ to $-0.13a_0$. Therefore, in moving the generalized transition state from the saddle point toward reactants the energy levels for the stretching and bending vibrational degrees of freedom increase and the rotational energy levels decrease. The stretching degree of freedom has the greatest contribution to the ratio $k^{\ddagger}(T)/k^{CVT}(T)$.

The H + HO reaction has its saddle point situated toward the asymptotic products region, $n_{AB}^{\ddagger} = 0.62$. As compared to the C + H_2 reaction the saddle point is further from the corner in the H + HO reaction and it is in a region of the potential energy surface where the stretching vibrational frequency is not as rapidly varying as in the C + H_2 or symmetric reactions. As for C + H_2 the stretching degree of freedom favors locating the variational transition state in a direction away from the corner, i.e., in the direction of increasing vibrational frequency which is toward products for the H + HO reaction. Both the bending and rotational degrees of freedom favor locating the transition state on the reactant side of the saddle point, but the bending vibrational frequency and the moment of inertia are slowly varying functions of s near the saddle point. Thus the stretching degree of freedom dominates the entropic considerations for the location of the transition state, and $s_*^{CVT}(T)$ is positive. At 200, 600, and 2400 K $s_*^{CVT}(T) = 0.15, 0.14$, and $0.09a_0$, respectively. For these shifts of the generalized transition state from the saddle point location, $s = 0$, the stretching vibrational frequency increases by 480, 440, and 300 cm^{-1}, respectively, the bending vibrational frequency decreases by 20, 17, and 10 cm^{-1}, respectively, and the moment of inertia increases by 6, 5, and 3%, respectively. It is interesting that the CVT transition state moves closer to the saddle point with increasing temperature. This is due to the competition between the stretching degree of freedom and the bending and rotational degrees of freedom. At low temperatures the quantal behavior of the stretching vibrational partition function allows the stretching degree of freedom to have the dominant entropic effect on the location of the variational transition state. However, as temperature increases the bending and rotational degrees of freedom becomes more important and tend to move the CVT transition state back toward the saddle point.

The H + HF reaction has a high endoergicity and its saddle point is in the asymptotic product valley at $n_{AB}^{\ddagger} = 0.91$. The stretching vibrational frequency is within 3% of its asymptotic product value and it is a slowly varying function of s compared to that for the four previously considered reactions near their saddle points. For the H + HF reaction the saddle point is a much looser transition state than for the H + HO or C + H_2 reactions. In the transition-state regions of the potential energy surfaces the bending vibrational frequency varies more rapidly in the H + HF system than in the others, and its rate of change is comparable to the rate of change of the stretching frequency. In moving the generalized transition state from the saddle point toward reactants the stretching vibrational frequency decreases, the bending vibrational frequency increases, and the moment of inertia decreases. As in the H + HO reaction, for H + HF the stretching degree of freedom and the bending and rotational degrees of freedom favor locations of the CVT transition state in opposite directions from the saddle point. However, the bending and rotational degrees of freedom dominate in the H + HF reaction and the CVT transition states are located at $s_*^{CVT}(T) = -0.1, -0.2$, and -0.5 for 200, 600, and 2400 K. At these locations of the CVT transition state the stretching frequency is 25, 55, and 180 cm^{-1} lower, respectively, than at the saddle point, the bending frequency is 22, 44, and 100 cm^{-1} higher, respectively, than at the saddle point, and the moment of inertia is 4, 7, and 17% lower than the saddle point value. In moving the generalized transition state from the saddle point to $s_*^{CVT}(T)$ the change in the frequency of the bending vibration is slightly smaller than that for the stretching vibration; however, the percent change in the partition function for the bend is larger than that for the stretch. This is primarily due to the fact that the bending partition function enters the rate constant expression as a square term. A secondary effect is that the bending degree of freedom behaves more classically than the stretching degree of freedom because the bending frequency is much lower than the stretching frequency, $\omega_e(s = 0) = 4279\ cm^{-1}$ and $\omega_b(s = 0) = 488\ cm^{-1}$. Therefore the partition function ratio for the bends is a more rapidly increasing function of temperature. The H + HF reaction is one of only three reactions in which the ratio $Q_{str}^{\ddagger}(T)/Q_{str}^{CVT}(T)$ of partition functions for the stretch is less than unity.

The last five figures (Figures 6–10) show free-energy curves for the endothermic reactions Li + HO, Cl + HO, Cl + HF, Li + HI, and I + Br, which have increasing AB bond order at the saddle point. This corresponds qualitatively to the saddle points becoming looser transition states, i.e., being located further into the relatively high-energy asymptotic product valley. For all five systems at all temperatures studied, the maxima in the free-energy curves and hence the CVT transition states are located on the reactant side of the saddle point and all three partition function ratios $Q^{\ddagger}(T)/Q^{CVT}(T)$ are greater than unity. This indicates that all three entropic effects—those of the bends, rotation, and the stretch—tend to move the transition state back toward reactants. For systems with loose conventional transition states like those for these systems, one can expect quite generally that making the generalized transition state tighter increases the bending restoring forces and decreases the moment of inertia thereby decreasing the partition functions for these two degrees of freedom. It is interesting that for all five systems the BEBO method predicts that the stretching vibrational energy levels also increase as the generalized transition state becomes tighter. However, in the asymptotic product valley the stretching vibrational frequency is only slowly varying, and the bending degree of freedom has more influence on the location of the variational transition state than the stretching or rotational degrees of freedom do. For a series of reactions at a given temperature, the partition function ratio $Q^{\ddagger}(T)/Q^{CVT}(T)$ tends to increase for bends and rotations and to decrease for stretches as the conventional transition state becomes looser.

The CVT transition state becomes less product-like as temperature increases in the range 200–2400 K for all five

reactions. This is because the energetic factor, $\exp[\Delta V^{CVT}(T)/k_BT]$, is an increasing function of temperature for a constant negative value of ΔV^{CVT}. The Boltzmann factor involving this quantity is the only factor favoring location of the variational transition state at the saddle point, and as temperature increases its effect diminishes allowing $s_*^{CVT}(T)$ to move further from the saddle point toward reactants for these five systems. However, the location of the CVT transition state can only be shifted from the saddle point as far as the corner of the reaction coordinate. At this location both the potential and the stretching vibrational frequency drop severely. The dip in the latter causes the sharp minima that are seen in the free-energy curves. For the less endoergic reactions Cl + HO, Li + HI, and I + HBr $s_*^{CVT}(T)$ (2400 K) is just on the product side of this minima in the free-energy curve.

It is also noted that for all five of the systems in Figures 6-10 the ratio $k^{\ddagger}(T)/k^{CVT}(T)$ is an increasing function of temperature. This is due to the fact that $k^{\ddagger}(T)/k^{CVT}(T)$ is dominated by the more classical degrees of freedom, i.e., the bending and rotational degrees of freedom. For such cases the ratio of conventional and CVT rate constants can be approximated by

$$\frac{k^{\ddagger}(T)}{k^{CVT}(T)} \underset{T\to\infty}{\sim} e^{\Delta V_b^{CVT}(T)/k_BT} \times \frac{I(s=0)}{I[s=s_*^{CVT}(T)]} \frac{\omega_b[s=s_*^{CVT}(T)]}{\omega_b(s=0)} \quad (86)$$

Both ratios on the right-hand side are greater than unity and increase as the temperature increases; thus the variational transition state moves further from the saddle point. In addition, the Boltzmann factor increases with temperature for constant negative ΔV_b^{CVT} indicating that the ratio of rate constants is an increasing function of temperature.

Finally, it is instructive to compare two of the five reactions in more detail. For this purpose we choose the reactions Cl + HO and Li + HI. The Cl + HO system has a smaller endoergicity, 8.3 kcal/mol as compared to 17.9 kcal/mol for Li + HI, and the latter reaction has its saddle point further into the asymptotic product valley. Although the saddle point is a looser transition state for Li + HI than for Cl + HO, the systems have remarkably similar saddle point bending frequencies, 172 and 171 cm^{-1}. The major difference between the two systems is due to the differences in the potential energy along the minimum energy path. In both reactions the potential rises sharply as the reaction coordinate turns the corner. Since the Li + HI reaction has its saddle point further into the asymptotic product valley than Cl + HO does, this sharp rise occurs further from the saddle point for Li + HI. The potential along the minimum energy path varies less than 10% as far as $s = -1.8a_0$ for the Li + HI reaction, whereas a 10% variation occurs already by $s = -0.8a_0$ for the Cl + HO reaction. At low temperatures the Boltzmann factor $\exp[\Delta V^{CVT}(T)/k_BT]$ is very sensitive to small changes in the potential and causes the generalized transition states to be near the saddle point for both systems; at 200 K $s_*^{CVT}(T) = -0.35a_0$ and $-0.30a_0$ for Cl + HO and Li + HI, respectively. The CVT transition state at 200 K is farther from the saddle point for the Cl + HO reaction than for the Li + HI reaction and the bending vibrational frequency changes more in the former case. Thus the partition function ratio $Q_b^{\ddagger}(T)/Q_b^{CVT}(T)$ is larger in the Cl + HO reaction than in the Li + HI reaction. At higher temperatures the Boltzmann factor allows for larger shifts in the variational transition state from the saddle point and thereby for larger changes in the potential. The Li + HI reaction has the CVT transition state much more displaced from the saddle point than Cl + HO does; for Cl + HO and Li + HI at 600 K, $s_*^{CVT}(T) = -0.50a_0$ and $-0.60a_0$, respectively, and at $T = 2400$ K $s_*^{CVT}(T) = -0.75a_0$ and $-1.40a_0$, respectively. The bending potential increases much more in going from the saddle point to $s_*^{CVT}(T)$ in the Li + HI reaction, and thus the partition function ratio for bends is larger in the Li + HI reaction above 300 K. Similarly the change in the moment of inertia in varying the generalized transition state is comparable in the two systems at 200 K, but becomes greater for Li + HI at higher temperatures. Thus the ratio of partition functions for rotation is also larger for the Li + HI reaction at all but 200 K. Similar considerations involving the stretching degree of freedom explain the fact that the ratio $Q_{str}^{\ddagger}(T)/Q_{str}^{CVT}(T)$ is larger for Li + HI than for Cl + HO.

We have seen that the dominant entropic effects on the location of the variational dividing surface are due to the stretching degree of freedom for symmetric conventional transition states and to the bending degree of freedom for relatively loose conventional transition states. The former effect tends to make the variational dividing surface less symmetric; the latter tends to make it more symmetric. Systems with only intermediate asymmetry in their conventional transition states tend to have smaller net effects because of a cancellation of these two effects.

Conclusion

We have used the BEBO method to generate a series of 36 reasonable potential energy surfaces for hydrogen atom transfer reactions. Using this set of surfaces we have calculated thermal reaction rates using conventional transition-state theory and canonical variational theory, both with quantized energy levels including anharmonicity. The conventional theory predicts rates higher than the variational theory by a median factor of 1.65 at 300 K and 2.0 at 2400 K. In some cases the factor is dramatically larger, such as for symmetric reactions, even those with high barriers. This may seem surprising because energetic factors might be expected to dominate entropic factors whenever the barrier is high. However, the decrease of the transverse stretching frequency near symmetric geometries predicted by the present BEBO formalism is so important that entropic factors may dominate the effects of even high barriers. Thus a high barrier alone is insufficient to guarantee the validity of conventional transition-state theory. Provided that tunneling is either unimportant or well accounted for, it can be argued both on the basis of the classical variational bound[7,10] and on the basis of our collinear tests[12] that, when the two theories differ, the canonical variational prediction is the more reliable one. We have considered several of the reactions in greater detail to illustrate the competition or reinforcement, as the case may be, of the energetic and the various entropic factors in determining the position of the maximum free energy of activation and in determining the magnitude and temperature dependence of the ratio of rate constants predicted by the two theories. In addition to the symmetric and nearly symmetric cases mentioned already in this paragraph, we find large effects for relatively loose transition states (the relatively loose generalized activated complexes considered here are not so loose that rotation of a diatomic fragment is free or nearly free). For cases with relatively loose transition states the most important factor decreasing the rate calculated with the variational dividing surface is due to the bending degree of freedom.

In most cases, when transition-state theory is used to interpret laboratory data, the comparison of transition-state theory to experiment is used to estimate at least one parameter of the potential energy surface, e.g., the classical barrier height or the vibrationally adiabatic barrier height. If transition-state theory predicts the rate for a given surface inaccurately, then the surface parameters so determined will be correspondingly inaccurate. Since the canonical variational prediction depends on the whole potential energy surface, as opposed to just the saddle point vicinity in the conventional theory, it is less

straightforward to use it to interpret experiments in terms of a small number of structural parameters. The simplest way to do this is to use a family of parametrized surfaces rather than let the parameters be saddle point properties as can be done with the conventional theory. When the canonical variational prediction of the rate differs from the conventional transition-state theory one for a surface estimated in any fashion, it at the least suggests that the conventional theory's predictions are unreliable for that system. It is still a formidable or impossible task to calculate thermal rate constants for most systems by accurate quantal scattering theory;[47] therefore canonical variational theory appears to be the best available practical theory for the calculation of gas-phase reaction rate constants.

References and Notes

(1) Johnston, H. S. "Gas Phase Reaction Rate Theory", Ronald Press: New York, 1966.
(2) Bunker, D. L. "Theory of Gas Phase Reaction Rates", Pergamon Press: Oxford, 1966.
(3) Laidler, K. J. "Theories of Chemical Reaction Rates", McGraw-Hill: New York, 1969.
(4) Benson, S. W. "Thermochemical Kinetics", 2nd ed.; Wiley: New York, 1976.
(5) Wigner, E. *Trans. Faraday Soc.* **1938,** 34, 29.
(6) Miller, W. H. *J. Chem. Phys.* **1975,** *62,* 1899.
(7) Pechukas, P. In "Dynamics of Molecular Collisions," Part B; Miller, W. H., Ed.; Plenum Press: New York, 1976; p 269.
(8) Keck, J. C. *Adv. Chem. Phys.* **1967,** *13,* 85.
(9) Pollak, E.; Pechukas, P. *J. Chem. Phys.* **1978,** *69,* 1218.
(10) Garrett, B. C.; Truhlar, D. G. *J. Phys. Chem.* **1979,** *83,* 1052.
(11) Chapman, S.; Hornstein, S. M.; Miller, W. H. *J. Am. Chem. Soc.* **1975,** *97,* 892.
(12) Garrett, B. C.; Truhlar, D. G. *J. Phys. Chem.* **1979,** *83,* 1079.
(13) See also Tweedale, A.; Laidler, K. J. *J. Chem. Phys.* **1970,** *53,* 2045. Wong, W. H.; Marcus, R. A. *ibid.* **1971,** *55,* 5625. Troe, J.; Quack, M. *Ber. Bunsenges. Phys. Chem.* **1974,** *78,* 240.
(14) Truhlar, D. G.; Kupperman, A. *J. Chem. Phys.* **1972,** *56,* 2232. Truhlar, D. G.; Kuppermann, A.; Adams, J. T. *ibid.* **1973,** *59,* 395. Baer, M.; Halavee, U.; Persky, A. *ibid.* **1974,** *61,* 5122. Truhlar, D. G.; Kuppermann, A.; Dwyer, J. *Mol. Phys.* **1977,** *33,* 683. Gray, J. C.; Truhlar, D. G.; Clemens, L.; Duff, J. W.; Chapman, F. M., Jr.; Morrell, G. O.; Hayes, E. F. *J. Chem. Phys.* **1978,** *69,* 240. Schatz, G. C.; Bowman, J. M.; Dwyer, J.; Kuppermann, A. Unpublished. Gray, J. C.; Garrett, B. C.; Truhlar, D. G. Unpublished.
(15) For a review, see Truhlar, D. G. *J. Phys. Chem.* **1979,** *83,* 188.
(16) Johnston, H. S.; Parr, C. A. *J. Am. Chem. Soc.* **1963,** *85,* 2544.
(17) The relation of variational theories to minimum density of states formalisms is discussed in Garrett, B. C.; Truhlar, D. G. *J. Chem. Phys.*, **1979,** *70,* 1593.
(18) Rapp, D.; Weston, R. E. *J. Chem. Phys.* **1962,** *36,* 2807. Schlag, E. W. *ibid.* **1963,** *38,* 2480. Laidler, K. J.; Polanyi, J. C. *Prog. React. Kinet.* **1965,** *3,* 1. Schlag, E. W.; Haller, G. L. *J. Chem. Phys.* **1965,** *42,* 584. Bishop, D. M.; Laidler, K. J. *ibid.* **1965,** *42,* 1688.
(19) Weston, R. E.; Schwarz, H. A. "Chemical Kinetics", Prentice-Hall: Englewood Cliffs, N.J., 1972; p 101.
(20) Parr, C. A., Ph.D. Thesis, California Institute of Technology, Pasadena, 1968.
(21) Garrett, B. C.; Truhlar, D. G. *J. Phys. Chem.*, in press.
(22) Wilson, E. B.; Decius, J. C.; Cross, P. C. "Molecular Vibrations", McGraw-Hill: New York, 1955.
(23) Truhlar, D. G. *J. Mol. Spectrosc.* **1971,** *38,* 415.
(24) Wigner, E. *Z. Phys. Chem., Abt. B* **1932,** *19,* 203.
(25) Garrett, B. C.; Truhlar, D. G. *J. Phys. Chem.* **1979,** *83,* 200.
(26) Johnston, H. S. *Adv. Chem. Phys.* **1961,** *3,* 131.
(27) Johnston, H. S.; Goldfinger, P. *J. Chem. Phys.* **1962,** *37,* 700.
(28) Mayer, W. S.; Schieler, L.; Johnston, H. S. *J. Chem. Phys.* **1966,** *45,* 385.
(29) Jordan, R. M.; Kaufman, F. *J. Chem. Phys.* **1975,** *63,* 1691. Dixon, D. A.; Herschbach, D. R. *Faraday Discuss. Chem. Soc.* **1977,** *62,* 166.
(30) Truhlar, D. G. *J. Am. Chem. Soc.* **1972,** *94,* 7584.
(31) Kafri, O.; Berry, M. J. *Faraday Discuss. Chem. Soc.* **1977,** *62,* 127.
(32) Rosen, B. "Spectroscopic Data Relative to Diatomic Molecules", Pergamon Press: New York, 1970.
(33) Krauss, M. *Natl. Bur. Stand. (U.S.) Tech. Note* **1967,** *No. 438.*
(34) "JANAF Thermochemical Tables", Stull, D. R., Ed.; Dow Chemical Co.: Midland, Mich., 1965.
(35) Marcus, R. A. *Discuss. Faraday Soc.* **1968,** *44,* 7. Harms, S. H.; Wyatt, R. E. *J. Chem. Phys.* **1975,** *62,* 3162, 3173. Elkowitz, A. B.; Wyatt, R. E. *ibid.* **1975,** *63,* 702. Redmon, M. J.; Wyatt, R. E. *Int. J. Quantum Chem., Symp.* **1975,** *9,* 403. **1977,** *11,* 343. Harms, S. H.; Elkowitz, A. B.; Wyatt, R. E. *Mol. Phys.* **1976,** *31,* 177.
(36) Quack, M.; Troe, J. *Ber. Bunsenges. Phys. Chem.* **1974,** *78,* 240. **1975,** *79,* 170, 469.
(37) Slater, J. C.; Kirkwood, J. G. *Phys. Rev.* **1931,** *37,* 682.
(38) Hirshfelder, J. O.; Curtiss, C. F.; Bird, R. B. "Molecular Theory of Gases and Liquids", Wiley: New York, 1964; p 987.
(39) Atomic polarizabilities were obtained from Miller, T. M.; Bederson, B. *Adv. At. Mol. Phys.* **1977,** *13,* 1. Diatomic polarizabilities were approximated by adding the polarizabilities of the two atoms. Dipole moments were obtained from Nelson, R.; Lide, D. R., Jr.; Maryott, A. "Selected Values of Electric Dipole Moments for Molecules in the Gas Phase", *Natl. Stand. Ref. Data Ser., Natl. Bur. Stand.* **1967,** *No. 10.* Phelps, D. H.; Dalby, F. W. *Phys. Rev. Lett.* **1966,** *16,* 3. Cade, P. E.; Huo, W. M. *J. Chem. Phys.* **1966,** *45,* 1063. Powell, F. X.; Lide, D. R., Jr. *Ibid.* **1965,** *42,* 4201.
(40) Gorin, E. *Acta Physicochim. URSS* **1938,** *9,* 681.
(41) Truhlar, D. G.; Olson, P. C.; Parr, C. A. *J. Chem. Phys.* **1972,** *57,* 4479.
(42) Bender, C. F.; Garrison, B. J.; Schaefer, H. F., III. *J. Chem. Phys.* **1975,** *62,* 1188.
(43) Klein, F. S.; Persky, A.; Weston, R. E. *J. Chem. Phys.* **1964,** *41,* 1799. Klein, F. S.; Persky, A. *ibid.* **1973,** *59,* 2775. Thompson, D. L.; Suzukawa, H. H. Jr.; Raff, L. M. *ibid.* **1975,** *62,* 4727.
(44) Truhlar, D. G.; Kuppermann, A. *J. Chem. Phys.* **1972,** *56,* 2232.
(45) Stern, M. J.; Persky, A.; Klein, F. *J. Chem. Phys.* **1973,** *58,* 5697. Baer, M. *Mol. Phys.* **1974,** *27,* 1429.
(46) Raff, L. M.; Stivers, L.; Porter, R. N.; Thompson, D. L.; Sims, L. B. *J. Chem. Phys.* **1970,** *52,* 3449.
(47) Schatz, G. C.; Kuppermann, A. *J. Chem. Phys.* **1976,** *65,* 4668.